Journal of Volcanology and Geothermal Research 354 (2018) 39–56

Contents lists available at ScienceDirect

Journal of Volcanology and Geothermal Research

journal homepage: www.elsevier.com/locate/jvolgeores

The onset of the volcanism in the Ciomadul Volcanic Dome Complex (Eastern Carpathians): Eruption chronology and magma type variation

Kata Molnár [a,*], Szabolcs Harangi [a,b], Réka Lukács [b], István Dunkl [c], Axel K. Schmitt [d], Balázs Kiss [b], Tamás Garamhegyi [e], Ioan Seghedi [f]

[a] Department of Petrology and Geochemistry, Eötvös Loránd University, Pázmány Péter stny. 1/c, H-1117 Budapest, Hungary
[b] MTA-ELTE Volcanology Research Group, Budapest, Hungary
[c] Sedimentology and Environmental Geology, Geoscience Centre, Georg-August University, Göttingen, Germany
[d] Institute of Earth Sciences, Ruprecht-Karls University, Heidelberg, Germany
[e] Department of Physical and Applied Geology, Eötvös Loránd University, Budapest, Hungary
[f] Institute of Geodynamics, Romanian Academy, Bucharest, Romania

ARTICLE INFO

Article history:
Received 29 June 2017
Received in revised form 9 January 2018
Accepted 29 January 2018
Available online 3 February 2018

Keywords:
Zircon (U-Th)/He dating
Eruption chronology
U-series dating
Quaternary
Harghita
Carpathian-Pannonian region

ABSTRACT

Combined zircon U-Th-Pb and (U-Th)/He dating was applied to refine the eruption chronology of the last 2 Myr for the andesitic and dacitic Pilişca volcano and Ciomadul Volcanic Dome Complex (CVDC), the youngest volcanic area of the Carpathian-Pannonian region, located in the southernmost Harghita, eastern-central Europe. The proposed eruption ages, which are supported also by the youngest zircon crystallization ages, are much younger than the previously determined K/Ar ages. By dating every known eruption center in the CVDC, repose times between eruptive events were also accurately determined. Eruption of the andesite at Murgul Mare (1865 ± 87 ka) and dacite of the Pilişca volcanic complex (1640 ± 37 ka) terminated an earlier pulse of volcanic activity within the southernmost Harghita region, west of the Olt valley. This was followed by the onset of the volcanism in the CVDC, which occurred after several 100s kyr of eruptive quiescence. At ca. 1 Ma a significant change in the composition of erupted magma occurred from medium-K calc-alkaline compositions to high-K dacitic (Baba-Laposa dome at 942 ± 65 ka) and shoshonitic magmas (Malnaş and Bixad domes; 964 ± 46 ka and 907 ± 66 ka, respectively). Noteworthy, eruptions of magmas with distinct chemical compositions occurred within a restricted area, a few km from one another. These oldest lava domes of the CVDC form a NNE-SSW striking tectonic lineament along the Olt valley. Following a brief (ca. 100 kyr) hiatus, extrusion of high-K andesitic magma continued at Dealul Mare (842 ± 53 ka). After another ca. 200 kyr period of quiescence two high-K dacitic lava domes extruded (Puturosul: 642 ± 44 ka and Balvanyos: 583 ± 30 ka). The Turnul Apor lava extrusion occurred after a ca. 200 kyr repose time (at 344 ± 33 ka), whereas formation of the Haramul Mic lava dome (154 ± 16 ka) represents the onset of the development of the prominent Ciomadul volcano. The accurate determination of eruption dates shows that the volcanic eruptions were often separated by prolonged (ca. 100 to 200 kyr) quiescence periods. Demonstration of recurrence of volcanism even after such long dormancy has to be considered in assessing volcanic hazards, particularly in seemingly inactive volcanic areas, where no Holocene eruptions occurred. The term of 'volcanoes with Potentially Active Magma Storage' illustrates the potential of volcanic rejuvenation for such long-dormant volcanoes with the existence of melt-bearing crustal magma body.

1. Introduction

Constraining eruption chronology has a primary importance in assessing volcanic hazards, since it provides information about the frequency of eruptions and the length of the repose time. Databases such as the Smithsonian's Global Volcanism Program collect available data primarily for the Holocene volcanic activity (Siebert et al., 2011). On the contrary, there is much less knowledge on volcanoes with known eruptions >10 kyr and possibly long repose times between active phases. Therefore, it is not easy to evaluate whether these volcanoes can be reactivated after prolonged quiescence or have become extinct (Connor et al., 2006). The poor knowledge about the nature of such long-dormant volcanoes is partly due to the difficulties to apply appropriate geochronometers, which can be used to accurately determine the eruption ages for the last 1 Myr.

Over the last decade, combined application of U-Pb or U-Th and (U-Th)/He zircon geochronology has become a promising method to date volcanic eruptions occurring during the second half of Pleistocene epoch (e.g., Schmitt et al., 2006, 2010; Danišík et al., 2012, 2017;

* Corresponding author.
E-mail address: molnar.kata@atomki.mta.hu (K. Molnár).

https://doi.org/10.1016/j.jvolgeores.2018.01.025

Harangi et al., 2015a; Mucek et al., 2017). This technique is proved to be particularly applicable when other dating methods such as radiocarbon, K/Ar or $^{40}Ar/^{39}Ar$ techniques encounter analytical or interpretational difficulties often caused by a lack of appropriate materials for dating (Danišík et al., 2017). Rapid temperature decrease below the ~200 °C closure temperature for He diffusion in zircon enables determination of eruption ages based on the (U-Th)/He systematics, assuming that no subsequent heating occurred (Farley, 2002).

The youngest volcanic activity of the Carpathian-Pannonian region occurred at Ciomadul volcano (Eastern Carpathians, Romania; Fig. 1). Although, its youngest eruption is dated at ca. 30 ka (Vinkler et al., 2007; Harangi et al., 2010, 2015a; Karátson et al., 2016) the composition and flux of the emitted gases at mofettas (Vaselli et al., 2002; Kis et al., 2017), seismic tomography (Popa et al., 2012) as well as combined petrologic and magnetotelluric studies (Kiss et al., 2014; Harangi et al., 2015b) indicate that there is still melt-bearing magma body beneath the volcanic complex and therefore, there is still a potential for further volcanic activity at Ciomadul (Szakács et al., 2002; Harangi, 2007; Szakács and Seghedi, 2013). Thus, there is a requirement for an accurate knowledge on the eruption behavior of the volcanic system. The timing of the last explosive eruptions and the chronology of the latest volcanic phase was determined by several authors (i.e., Moriya et al., 1995, 1996; Vinkler et al., 2007; Harangi et al., 2010, 2015a; Karátson et al., 2016). In this paper, we focus on the older history, i.e., the onset of the volcanism at the Ciomadul Volcanic Dome Complex (cf. Szakács et al., 2015), which comprises the volcanic edifice of Ciomadul and the peripheral lava domes. Based on previous K/Ar ages (Peltz et al., 1987; Pécskay et al., 1995; Szakács et al., 2015) the peripheral domes are considered to have formed between 2 and 0.5 Ma. Here, we adopted the methodology used by Schmitt et al. (2006), Danišík et al. (2012) and Harangi et al. (2015a), where they determined eruption ages from combined U-Th and (U-Th)/He zircon dating. Individually, these chronometers yield independent constraints on crystallization and eruption ages, but because zircon crystallization always precedes eruption, the combined methods allows for an independent check of the accuracy of the dating. The eruption ages were combined by newly analyzed major and trace element compositional data allowing the evaluation of chemical changes in the erupted magmas. These data yield important new information about the nature of a little known long-dormant volcano in eastern-central Europe.

2. Geological background

The Călimani-Gurghiu-Harghita volcanic chain (CGH) is located in the southeastern part of the Carpathian-Pannonian region (CPR), eastern-central Europe (Fig. 1). The CPR comprises the Pannonian basin characterized by thin continental crust and lithosphere surrounded by orogenic mountain belts of the Alps, Carpathians and Dinarides (e.g., Horváth et al., 2006). Major thinning of the lithosphere has been considered to be a result of the Early to Mid-Miocene retreating subduction of an oceanic lithosphere underneath at the Eastern Carpathians (e.g., Royden et al., 1983; Csontos et al., 1992; Horváth et al., 2006). The southeastern edge of the CGH is located ~50 km from the Vrancea zone that exhibits the largest present-day strain concentration in continental Europe (Wenzel et al., 1999; Ismail-Zadeh et al., 2012). This is due to a near-vertical slab descending into the upper mantle (Oncescu et al., 1984; Martin et al., 2006) that poses a persistent regional seismic hazard. The reason of the descending vertical lithospheric slab beneath Vrancea is strongly debated. Explanations involve as it represents the latest stage of the subduction along the Carpathians (Sperner et al., 2001), but lithospheric delamination in the absence of subduction (Fillerup et al., 2010; Koulakov et al., 2010) or a combination of lithospheric delamination and subduction roll-back have been alternatively proposed (Gîrbacea and Frisch, 1998; Girbacea et al., 1998; Chalot-Prat and Gîrbacea, 2000).

Volcanic activity of the South Harghita and the nearby Perşani alkali basalt volcanic field could be related to this active tectonic setting, although the link between the vertical slab movement, magma

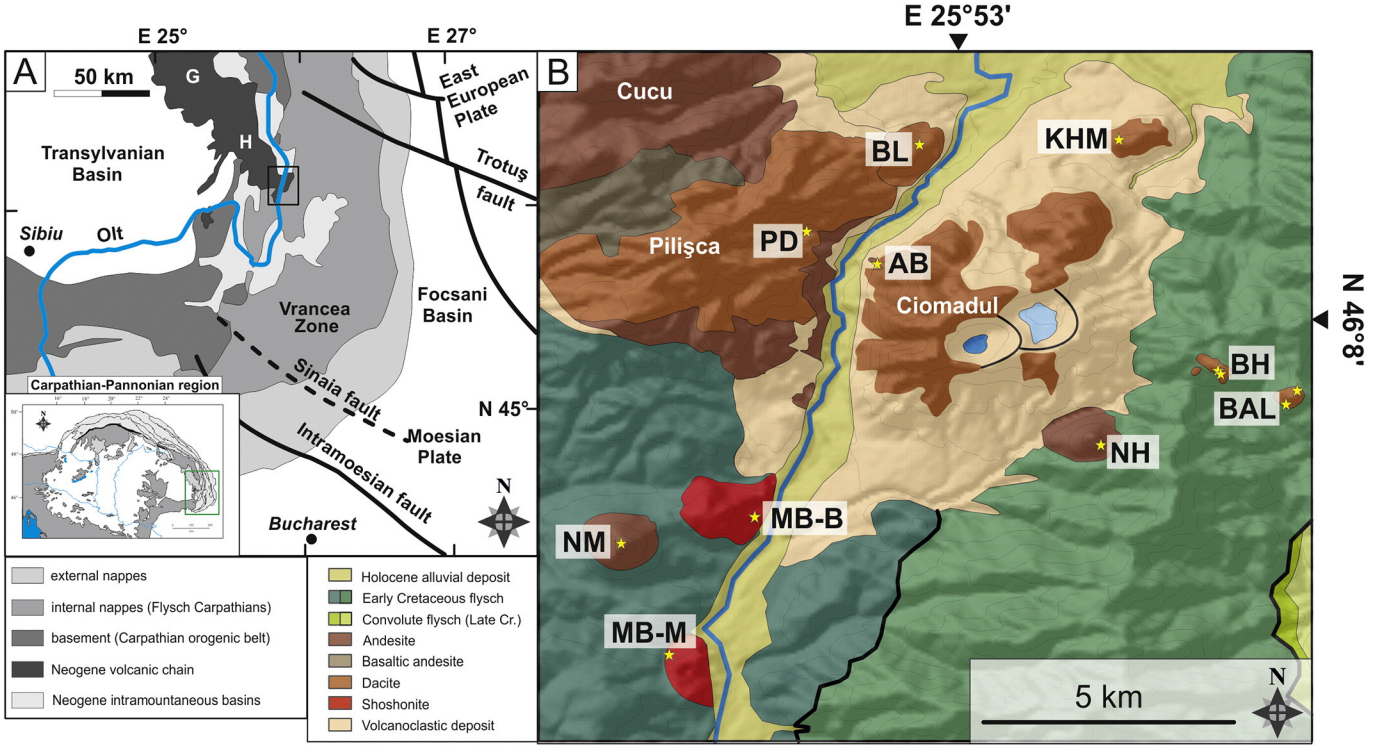

Fig. 1. (A) Simplified geological map about the location of the Călimani-Gurghiu-Harghita volcanic chain in the Carpathian-Pannonian region (modified after Cloetingh et al., 2004 and Harangi et al., 2013). The rectangle indicates the area of the South Harghita. (B) Geological map of the South Harghita with the sampling sites (based on the 1:200,000 map of Ianovici and Rădulescu, 1966, Geological Institute of Romania and Szakács et al., 2015). G: Gurghiu Mts., H: Harghita Mts.; PD: Pilişca, BL: Baba-Laposa, AB: Turnul Apor, KHM: Haramul Mic, BH: Puturosul, BAL: Balvanyos, NH: Dealul Mare, MB-M: Malnaş, MB-B: Bixad, NM: Murgul Mare.

generation, and volcanism is still unclear (Downes et al., 1995; Harangi et al., 2013; Seghedi et al., 2004, 2011, 2016).

In the CPR, eruptions of various magmas from basalt to rhyolite have occurred since 18 Ma (Szabó et al., 1992; Harangi, 2001; Konečný et al., 2002; Seghedi et al., 2004, 2011; Harangi and Lenkey, 2007; Seghedi and Downes, 2011). In the eastern part, volcanism occurred at the Călimani-Gurghiu-Harghita andesitic-dacitic volcanic chain from ca. 10.2 Ma onward and gradually shifted to the southeast with waning intensity (Peltz et al., 1987; Pécskay et al., 1995, 2006; Szakács et al., 1997). The CGH volcanism postdates the inferred subduction during the mid-Miocene (Cloetingh et al., 2004) and therefore is considered post-collisional (Mason et al., 1996; Seghedi et al., 1998; Seghedi and Downes, 2011). Volcanic activity in the South Harghita (Luci-Lazu, Cucu, Pilişca and Ciomadul; Fig. 1) started at 5.3 Ma (Pécskay et al., 1995) and was coeval with or slightly post-dated the subsidence of the nearby Braşov, Gheorgheni and Ciuc basins (Girbacea et al., 1998; Fielitz and Seghedi, 2005). After a gap between 3.9 and 2.8 Ma (Pécskay et al., 2006; Seghedi et al., 2011), a sharp compositional change occurred in the erupted magmas, which is reflected in the more potassic and incompatible element-enriched nature at Cucu, Pilişca and Ciomadul compared to earlier volcanism (Mason et al., 1996; Harangi and Lenkey, 2007; Seghedi et al., 2011). This transition spatially coincides with the southward migration of the volcanic centers across the Trotuş fault (Fig. 1). The Trotus fault tectonically separates the European and Moesian continental blocks, which corresponds to a decrease in crustal thickness from 40–45 km in the European to 35–40 km in the Moesian block (e.g., Cloetingh et al., 2004).

The southern, more potassic volcanism of South Harghita developed between 2.8 and 0.03 Ma and comprises the andesitic Cucu, the basaltic-andesitic, andesitic and dacitic Pilişca volcanoes and the andesitic and dacitic Ciomadul Volcanic Dome Complex (Casta, 1980; Peltz et al., 1987; Seghedi et al., 1987; Szakács et al., 1993, 2015; Pécskay et al., 1995, 2006; Fig. 1B; Table 1). Chemical composition of the chain end-member Ciomadul volcanics was interpreted to mark the transition from normal calc-alkaline to adakite-like magmas (Seghedi et al., 2011).

The Ciomadul Volcanic Dome Complex comprises the massive Ciomadul volcano and the surrounding peripheral lava domes (Dealul Mare, Haramul Mic, Puturosul and Balvanyos; Fig. 1B; Table 1) as defined by Szakács et al. (2015). However, we consider that the two shoshonitic domes at Malnaş and Bixad as well as the dacitic Baba-Laposa dome also belong to this volcanic system. The volcanic edifices were constructed on the Cretaceous Ceahlău-Severin flysch nappe and are bordered by the Plio-Pleistocene intramontane Lower Ciuc basin in the north (Fig. 1B). The youngest phase of volcanism occurred at the Ciomadul volcano between ~56 and 32 ka based on radiocarbon, thermal luminescence and combined zircon U-Th and (U-Th)/He dating (e.g., Moriya et al., 1995, 1996; Vinkler et al., 2007; Harangi et al., 2010, 2015a; Karátson et al., 2016). It represents the youngest volcanic activity of the entire Carpathian-Pannonian region.

3. Samples and analytical methods

3.1. Sampling and whole-rock techniques

This study focuses mainly on the peripheral lava domes (Szakács et al., 2015) surrounding the central lava dome edifice of Ciomadul (Fig. 1B). They represent the older phase of the volcanism in the CVDC. We attempted to sample all the known eruptive centers in addition to sampling the youngest volcanic products of the nearby Pilişca volcano. Sample sites, names and lithology are listed in Table 1; the

Table 1
Sample names, localities, lithologies and previous age results of the studied samples from the southernmost Harghita. The corresponding Hungarian names of the locations are also indicated in italic.

Sample code in the text	Sample code (in the lab)	Location	GPS coordinates		Lithology	"Affiliation" and reference	Dated fraction	Age (Ma)	Method	Reference
			N	E						
NM	CSO-NM1	Murgul Mare - *Nagy Murgó*	46°4′ 36″	25°48′ 01″	Andesite	Pilişca - Panaiotu et al. (2012)	Whole rock	2.69 ± 0.22	K/Ar	Szakács et al. (2015)
							Whole rock	2.25 ± 0.09		
PD	CSO-PD2	Pilişca - *Piliske*	46° 9′ 16″	25°50′ 47″	Dacite	Pilişca - Seghedi et al. (1987)	Biotite	2.1 ± 0.1	K/Ar	Pécskay et al. (1995)
							Whole rock	1.8 ± 0.1	K/Ar	Pécskay et al. (1995)
							Biotite	1.5 ± 0.1	K/Ar	Pécskay et al. (1995)
MB-M	CSO-MB-M	Malnaş quarry - *Málnás*	46°2′ 59″	25°48′ 43″	Shoshonite	Distinct unit - Seghedi et al. (1987)	Whole rock	2.22 ± 0.14	K/Ar	Peltz et al. (1987)
								1.95–1.77	Palaeomagnetic	Panaiotu et al. (2012)
MB-B	CSO-MB-B	Bixad quarry - *Bükszád*	46°5′ 1″	25°50′ 1″	Shoshonite	Distinct unit - Seghedi et al. (1987)	Whole rock	1.45 ± 0.40	K/Ar	Peltz et al. (1987)
								1.95–1.77	Palaeomagnetic	Panaiotu et al. (2012)
BL	CSO-BL	Baba-Laposa - *Bába-Laposa*	46°10′ 33″	25°52′ 27″	Dacite	Pilişca - Szakács et al. (2015)	Whole rock	1.46 ± 0.27	K/Ar	Szakács et al. (2015)
NH	CSO-NH5	Dealul Mare - *Nagy-Hegyes*	46°6′ 06″	25°55′ 9″	Andesite	Ciomadul - Panaiotu et al. (2012)	Whole rock	1.02 ± 0.07	K/Ar	Szakács et al. (2015)
BH	CSO-BH	Puturosul - *Büdös-hegy*	46°7′ 11″	25°56′ 55″	Dacite	Ciomadul - Panaiotu et al. (2012)	Whole rock	0.71 ± 0.04	K/Ar	Szakács et al. (2015)
	CSO-BH(sz)		46°7′ 8″	25°56′ 56″						
BAL	MK-2	Cetatea Balvanyos - *Bálványos*	46°6′ 42″	25°57′ 53″	Dacite	Ciomadul - Panaiotu et al. (2012)	Whole rock	1.02 ± 0.15	K/Ar	Pécskay et al. (1995)
	CSO-BAL(cs)		46°6′ 54″	25°58′ 4″			Whole rock	0.92 ± 0.18	K/Ar	Pécskay et al. (1995)
AB	CSO-AB	Turnul Apor - *Apor-bástya*	46°8′ 6″	25°51′ 51″	Dacite	–	–	–	–	–
KHM	CSO-KHM1	Haramul Mic - *Kis-Haram*	46°10′ 38″	25°55′ 25″	Dacite	Ciomadul - Seghedi et al. (1987)	Whole rock	0.85	K/Ar	Casta (1980)

Hungarian names of each locality are also indicated due to the bilingual character of this part of Romania.

Petrology of the studied samples and textural characterization of zircon crystals were performed by combined investigation with petrographic microscope and an AMRAY 1830 type SEM + EDAX PV9800 EDS equipped with a GATAN MiniCL at the Department of Petrology and Geochemistry of the Eötvös Loránd University, Budapest, Hungary.

Whole-rock major and trace element geochemical compositions were analyzed at AcmeLabs (Vancouver, Canada; http://acmelab.com/). Major and minor elements were determined by ICP-emission spectrometry and trace elements were analyzed by ICP-MS following a lithium borate fusion and dilution in acid.

3.2. Zircon extraction

Approximately 1 kg of rock was collected from each outcrop. Samples were crushed and sieved, and the 63–125 μm fraction was gravity separated in heavy liquid (sodium polytungstate with a density of 2.88 ± 0.01 g/cm^3). Zircon was concentrated by removing Fe-Ti oxides using a permanent magnet. Inclusion- and fissure-free intact, euhedral zircon crystals >60 μm in width were hand-picked from the non-magnetic fraction under a binocular microscope, photographed and packed into platinum capsules for He degassing. For the petrographic and textural characterization of zircon populations, ~80 crystals per sample were hand-picked, mounted in a 2.54 cm epoxy disk and polished.

3.3. (U-Th)/He-analysis

(U-Th)/He age determinations were carried out at the GÖochron Laboratory of Georg-August University, Göttingen. Single-crystal aliquots were dated, usually six aliquots per sample. The Pt capsules were heated for 5 min (ca. 1200 °C) under high vacuum by an infrared laser and the extracted gas was purified using a SAES Ti-Zr getter at 450 °C. The chemically inert noble gases and a minor amount of other rest gases were then expanded into a Hiden triple-filter quadrupole mass spectrometer equipped with a positive ion counting detector. One or more "gas re-extract" steps were run for each sample to verify complete degassing of the crystals. The residual gas is usually around 1 to 2% after the first extraction. He gas results were corrected for blank, determined by heating empty Pt capsules using the same procedure.

Following degassing, zircon crystals were retrieved from the gas extraction line, extracted from the Pt capsules and spiked with calibrated ^{230}Th and ^{233}U solutions. The crystals were dissolved in pressurized Savillex teflon bombs using a mixture of double distilled 48% HF and 65% HNO_3 at 220 °C during 5 days. Spiked solutions were analyzed as 0.4 ml solutions by isotope dilution for ^{233}U, ^{235}U, ^{238}U, ^{230}Th, ^{232}Th and ^{147}Sm using a Perkin Elmer Elan DRC II ICP-MS with an APEX micro-flow nebulizer. Procedural U and Th blanks by this method are usually very stable in a measurement session and below 1.5 pg. Total analytical uncertainty (TAU) was computed as the square root of the sum of the squares of weighted uncertainties of U, Th, Sm and He measurements. The raw (U-Th)/He ages were adjusted according to the alpha ejection correction procedure (F_T) assuming homogeneous distribution of U and Th and using the base equations of Farley et al. (1996) and Farley (2002) and the tetragonal crystal model and fit parameters given by Hourigan et al. (2005). The individual (U-Th)/He ages were calculated by the Taylor Expansion Method (Braun et al., 2012). The TAU and the estimated error of F_T were used to calculate the uncertainties of F_T-corrected (U-Th)/He ages.

The accuracy of zircon (U-Th)/He dating was monitored by replicate analyses of the reference material of Fish Canyon Tuff zircon, yielding a mean (U-Th)/He age of 28.1 ± 2.3 Ma (n = 128; where n is the number of replicate analyses per sample) which consistent with the reference (U-Th)/He age of 28.3 ± 1.3 Ma (Reiners, 2005).

In order to perform initial Th disequilibrium correction for the (U-Th)/He ages, zircon crystals from all samples were dated by in-situ U-Th-Pb geochronology using LA-ICP-MS (ETH Zürich) and/or SIMS (HIP laboratory, University of Heidelberg) methods. Analytical backgrounds and results are presented in Lukács et al. (submitted). In case of the KHM sample (the youngest sample dated in this study), double-dating was also conducted, i.e., after in-situ SIMS analysis, 4 zircon crystals from the indium mount were picked out, cleaned by cc. HCl and analyzed for (U-Th)/He ages.

4. Results

4.1. General petrography and geochemistry

The studied lava dome rocks comprise andesites (SiO_2 = 58–62 wt%) and dacites (SiO_2 = 63–67 wt%; Fig. 2A) with calc-alkaline, high-K calc-alkaline and shoshonitic composition (Table 2). Three groups can be distinguished based on their SiO_2 and K_2O contents (Fig. 2A) according to the classification of Peccerillo and Taylor (1976):

(1) medium-K calc-alkaline series (CAs) – Murgul Mare and Pilişca
(2) high-K calc-alkaline series (HKCAs) – Baba-Laposa, Haramul Mic, Puturosul, Balvanyos, Dealul Mare and Turnul Apor
(3) high-K calc-alkaline-shoshonitic series (HKSs) – Malnaş and Bixad.

The volcanic rocks are crystal-rich, porphyritic (phenocryst content is 25–40 vol%) with abundant glomerocrystic aggregates and crystal clots in a hyalopilitic to holocrystalline matrix. The phenocryst assemblage of the CAs and HKCAs samples invariably comprises plagioclase, amphibole and biotite. Additionally, clinopyroxene and rounded quartz are present in the Murgul Mare andesite (CAs), and clinopyroxene, orthopyroxene and olivine in the Turnul Apor dacite (HKCAs). The dominantly high-Mg character of these minerals and their occurrence in microenclaves, crystal clots, glomerocrysts and individual crystals are similar to the younger lava dome rocks of the Ciomadul volcano. The accessory phases are zircon and apatite, while the HKCAs samples contain additional titanite. Most of the samples have a fine-grained groundmass with plagioclase microlites, Fe-Ti oxides and SiO_2 batches except for the Murgul Mare andesite which has a coarse-grained groundmass.

The samples of the HKSs contain much fewer phenocrysts (5–10%) which comprise dominantly clinopyroxene and altered feldspar, whereas biotite, amphibole together with rounded quartz, orthopyroxene, olivine and titanite are present in minor amounts. In these rocks the groundmass is coarse-grained, containing dominantly feldspar and clinopyroxene microlites, the accessories are zircon, apatite and titanite. The mineral phases of both the HKCAs and HKSs samples together with the Murgul Mare sample (CAs) display diverse, disequilibrium textures similar to the HKCAs dacite of the Ciomadul volcano implying open system magma chamber processes involving mixing of distinct magmas (Kiss et al., 2014).

Earlier bulk rock geochemical data for the South Harghita volcanic formations were reported by Szakács and Seghedi (1986), Mason et al. (1996, 1998), Harangi and Lenkey (2007), Vinkler et al. (2007) and Seghedi et al. (2011). These were completed with new bulk rock compositional data (Appendix 1). Most of the volcanic rocks (HKSs and HKCAs) show enrichment of LIL (large ion lithophile; e.g., Cs, Rb, Ba, K, Sr) and depletion of HFS (high field strength; e.g., Nb, Ti) elements that are characteristic also of the youngest pumices of the Ciomadul volcano (Vinkler et al., 2007; Fig. 2C, D). They are particularly enriched in Sr and Ba (>1000 ppm), whereas another common feature is the absence of negative Eu anomaly (Eu/Eu* values ranging from 1.1 to 0.9). The three compositional groups are clearly separated in the Sr vs Sm/Yb plot (Fig. 2B). Furthermore, this plot illustrates also the distinct characters of the HKSs samples (Fig. 2B), possibly implying different

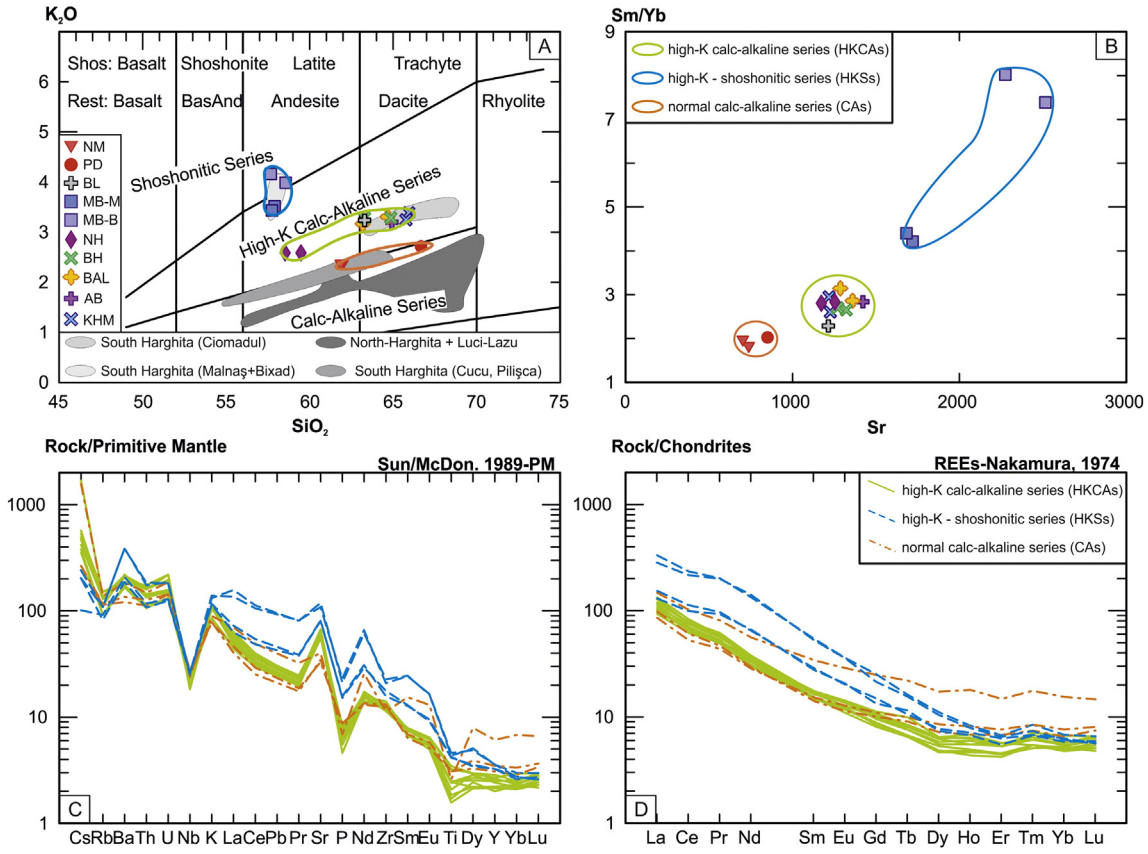

Fig. 2. Major and trace element variation diagrams (A and B) and trace element characteristics (C and D) of the studied samples. (A) SiO_2 vs K_2O classification diagram (the fields after Peccerillo and Taylor, 1976) for the studied rocks. The different grey fields indicate whole rock data from the Harghita for comparison from Mason et al. (1996) and Harangi and Lenkey (2007); (B) Sr vs Sm/Yb; (C) primitive mantle-normalized trace element plots and (D) chondrite-normalized REE plots (normalizing values after Sun and McDonough, 1989 and Nakamura, 1974, respectively).

proportions of the mixed magmas (Seghedi et al., 1987; Mason et al., 1996). The geochemical difference between the samples of Murgul Mare, Malnaş and Bixad is remarkable, since they occur in the same restricted area, very close to each other (Fig. 1B). The two CAs samples, i.e. the Murgul Mare and Pilişca are similar in Sr and Sm/Yb, but are distinct in other major and trace element character. The Murgul Mare andesite shows some geochemical similarities to the HKCAs, whereas the Pilişca dacite is clearly distinct and resembles the intermediate rocks of South Harghita (Mason et al., 1996).

4.2. Characteristics of zircon crystals

All of the studied samples contain zircon as accessory phase. The crystals occur as inclusions in the phenocrysts and in fewer amounts in the groundmass. All samples comprise dominantly euhedral crystals, but partially resorbed crystals are also present. Selected types of zircon grains shown in Fig. 3. In the CAs samples, and in most of the HKCAs samples euhedral crystals are dominating, whereas in the HKSs-samples and the HKCAs dacite of Puturosul and Balvanyos, zircon crystals are usually rounded. The dimensions of the studied zircons vary considerably (Table 3). Zircon crystals in samples Pilişca and Murgul Mare are the longest; they range from 320 to 780 μm and 130 to 620 μm, respectively, whereas the smallest crystals are in the Dealul Mare andesite, where the zircon size varies between 120 and 200 μm. In other samples, zircon crystals have a maximum length of 280 μm and a minimum length of 140 μm.

The average aspect ratio (length/width) is ~3:1, the most elongated crystals are in the samples of Pilişca and Balvanyos with an aspect ratio of ~5:1. Although the shape, size and appearance of the zircon crystals vary through the sample sets, their internal structure is uniform. They typically show oscillatory zoning in each sample which is sometimes accompanied by sector zoning (Fig. 3D).

Table 2
General petrological and geochemical features of the southernmost Harghita samples.

Arc rock-type	Lithology	Sample	Phenocryst assemblage	Accessories	SiO_2 (wt%)	K_2O (wt%)
Normal calc-alkaline	Andesite	NM	Plagioclase, amphibole, biotite, clinopyroxene, quartz	Zircon, apatite	61.8	2.4
	Dacite	PD	Plagioclase, amphibole, biotite	Zircon, apatite	66.6	2.7
High-K calc-alkaline	Andesite	NH	Amphibole, plagioclase, biotite, apatite	Zircon, apatite, titanite	58.9	2.6
	Dacite	BL	Plagioclase, biotite, amphibole, titanite	Zircon, apatite, titanite	63.2–65.8	3.2–3.3
		BH	Plagioclase, amphibole, biotite, apatite	Zircon, apatite, titanite		
		BAL	Plagioclase, biotite, amphibole,	Zircon, apatite, titanite		
		AB	Plagioclase, amphibole, biotite, clinopyroxene, orthopyroxene, olivine, titanite	Zircon, apatite, titanite		
		KHM	Plagioclase, biotite, amphibole, titanite	Zircon, apatite, titanite		
High-K/shoshonite	Andesite	MB-B	Clinopyroxene, feldspar, biotite, amphibole, quartz, orthopyroxene, olivine	Zircon, apatite, titanite	57.8–58.5	3.5–4.0
		MB-M	Clinopyroxene, feldspar, biotite, amphibole, quartz, orthopyroxene, olivine	Zircon, apatite, titanite		

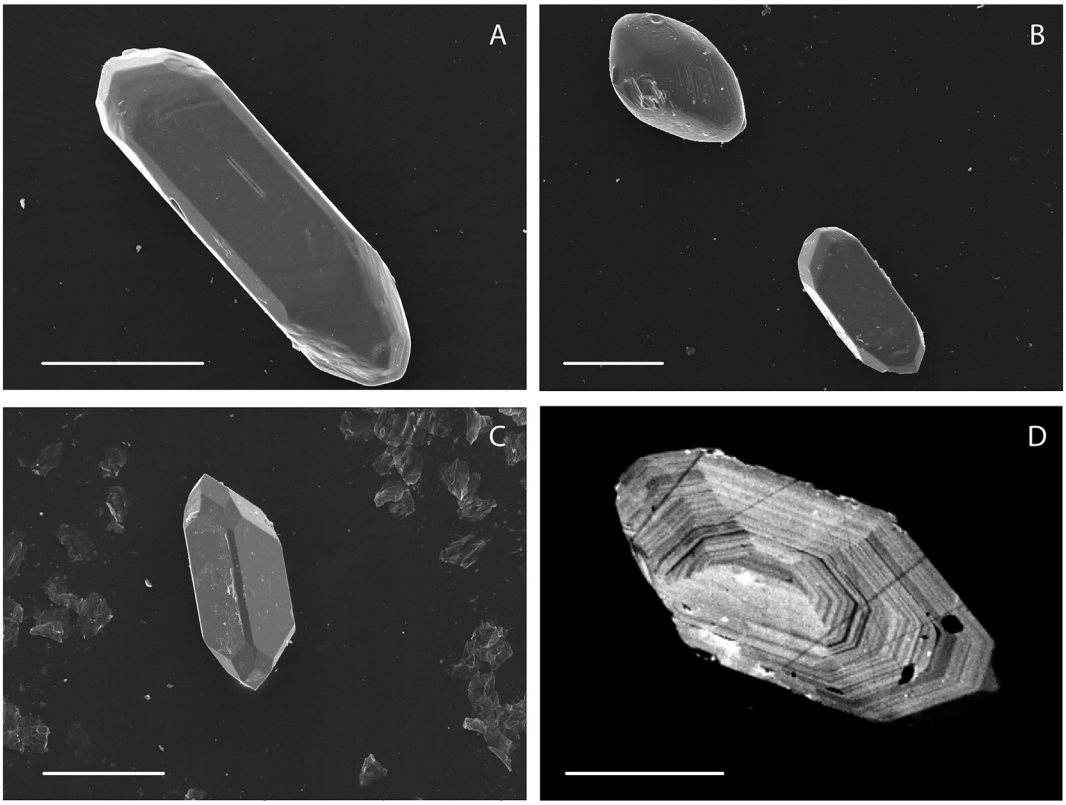

Fig. 3. Selected zircon types from the studied samples (A, B, C: SEM-SE images of intact crystals; D: cathodoluminescence image of sectioned crystal). The scale is 100 μm. (A) slightly resorbed (Balvanyos); (B) resorbed (upper) and euhedral (lower) crystal (Baba-Laposa); (C) euhedral crystal (Dealul Mare); (D) typical internal structure of zircon with oscillatory zoning accompanied occasionally by sector zoning (Murgul Mare).

In most cases, the boundaries between the zones are sharp; however, rounded ones indicating resorption can be also observed around the interior domains in some crystals. These cores have typically higher U concentrations (darker in CL images) and often contain thorite inclusions along the resorption boundary. The inclusion population in zircon crystals is quite uniform in all samples; apatite and glass inclusions are present in almost every crystal, whereas feldspar, amphibole, biotite, Fe-Ti oxide and thorite inclusions are subordinate.

4.3. Zircon (U-Th)/He data

Single-grain (U-Th)/He zircon geochronology was applied to constrain the eruption ages of the peripheral lava domes of the CVDC (Table 4). Data having high analytical uncertainties (>10%), low F_T values (<0.6) or unusually high U and Th content (implying the presence of inclusions) were not considered in further calculations. The distribution of the remaining dataset was tested for normality by using Q-Q-plots and Shapiro-Wilk test (Upton and Cook, 1996), which was confirmed for all samples except for two outliers in samples KHM. A relatively small scatter of the data is indicated by the mean square of weighted deviates (MSWD) of 0.1 to 2.0. MSWD values in excess of the accepted range of the distribution are explained by simplified assumptions regarding zircon crystal geometry, heterogeneous distribution of parent nuclides, the presence of minute inclusions with elevated actinide contents and other imperfections of the crystals affecting the accuracy of the F_T-correction (e.g., Danišík et al., 2012).

Table 3
Zircon sizes and aspect ratios (minimum, maximum and average) of the studied samples.

Sample	PD	BL	MB	NH	BH	BAL	AB	KHM	NM
Length (μm)									
Minimum	326	133	147	121	149	136	114	162	125
Maximum	783	283	508	302	285	336	227	272	618
Average	438	204	243	200	203	238	165	202	219
Aspect ratio									
Minimum	1.9	1.6	1.5	1.6	2.0	2.3	2.4	2.3	1.6
Maximum	5.1	3.6	4.3	3.9	3.9	5.6	4.2	3.3	4.6
Average	2.7	2.5	2.9	2.6	2.7	3.3	3.1	2.8	2.8

The obtained F_T-corrected (U-Th)/He single-grain zircon dates are between 2.07 and 0.11 Ma (Table 4 and Appendix 2). Zircon crystals from the CAs samples are the oldest where the age range of the zircon dates varies between 2070 and 1760 ka (n = 6) and from 1700 to 1590 ka (n = 5) for the andesitic Murgul Mare and the dacite of the Pilişca volcano, respectively. The age range of the two HKSs samples is overlapping, their single-grain dates vary between 1050 and 920 ka (n = 8) and 1030 and 780 ka (n = 8) for the Malnaş and Bixad, respectively. The HKCAs cover a wider age interval compared to the other two groups. The age range (1060–780 ka (n = 11)) of the Baba-Laposa which is oldest HKCAs sample overlaps with the HKSs samples. The single-grain dates of the andesitic Dealul Mare and the dacitic Puturosul and Balvanyos vary 880–810 ka (n = 6), 730–570 ka (n = 8) and 650–520 ka (n = 11), respectively. The two youngest samples among all of the dated units are the dacitic Turnul Apor and Haramul Mic, their age ranges vary between 340 and 310 ka (n = 3) and 170 and 110 ka (n = 12), respectively.

4.4. The effect of secular disequilibrium

(U-Th)/He dating is based on the ingrowth of ^{4}He under secular equilibrium from the ^{238}U, ^{235}U, ^{232}Th decay series and ^{147}Sm decay (Farley, 2002). However, due to the fractionation of the intermediate daughter isotopes (e.g., ^{230}Th, ^{226}Ra, ^{231}Pa), this condition is valid only after ~5 half-lives of the longest-lived fractionating intermediate nuclide (Farley et al., 2002). This corresponds to >380 kyr prior to eruption for the U-Th decay system and the expected fractionation of ^{230}Th

Table 4
Complete dataset of measurements, corrections, and calculations used to obtain final (U-Th)/He eruption ages.

Sample name	Sample ID	Sample code	^{232}Th (ng)	± %[a]	^{238}U (ng)	± %[a]	^{147}Sm (ng)	±%[a]	^{4}He (ncc)	±%[a]	TAU[b] (%)	Th/U	Raw (U-Th)/He age (ka)	±1 s.d. (ka)	F_T[c]	±[d] (%)	F_T-cor. (U-Th)/He age[e] (ka)	±1 s.d.[f] (ka)	D_{230}[g]	Disequilibrium corrected (U-Th)/He age[h] (ka)	+1σ[i] (ka)	−1σ[i] (ka)	±1σ[i] (ka)
Haramul Mic	KHM	CSO-KHM-1 z1	2.406	2.4	2.819	1.8	0.003	25.1	0.043	3.0	3.4	0.85	105.5	3.5	0.727	8.2	145.1	12.9	0.263	**178.9**	16.7	20.2	18.4
		CSO-KHM-1 z2	2.639	2.4	3.979	1.8	0.001	37.6	0.055	2.9	3.3	0.66	99.4	3.3	0.777	6.7	127.8	9.5	0.205	**154.3**	17.6	13.1	15.4
		CSO-KHM-1 z3	4.920	2.4	5.863	1.8	0.003	22.2	0.086	2.5	2.9	0.84	101.8	2.9	0.771	6.9	132.1	9.8	0.259	**158.6**	15.4	14.8	15.1
		CSO-KHM-1 z4[m]	7.437	2.4	4.666	1.8	0.003	26.5	0.146	2.1	2.6	1.59	187.9	4.8	0.747	7.6	251.7	20.2	0.492				
		CSO-KHM-1 z5	3.145	2.4	3.840	1.8	0.003	20.6	0.064	2.7	3.1	0.82	115.1	3.6	0.797	6.1	144.4	9.9	0.253	**177.4**	14.2	15.2	14.7
		CSO-KHM-1 z6	5.841	2.4	5.890	1.8	0.008	16.3	0.115	2.2	2.7	0.99	130.8	3.5	0.814	5.6	160.7	10.0	0.306	**194.3**	12.0	13.2	12.6
		CSO-KHM-1 z7[m]	1.478	2.4	1.643	1.8	0.006	24.3	0.034	3.2	3.5	0.90	142.1	5.0	0.747	7.6	190.2	15.9	0.278				
		CSO-KHM-1 z8[l]	2.459	2.4	2.895	1.8	0.013	12.7	0.073	22.1	22.2	0.85	174.7	38.7	0.723	8.3	241.5	57.2	0.262				
		CSO-KHM-1 z9[m]	6.436	2.4	5.143	1.8	0.024	10.7	0.118	2.2	2.6	1.25	147.0	3.9	0.777	6.7	189.3	13.6	0.386				
		CSO-KHM-1 z10	2.691	2.4	3.839	1.8	0.011	15.8	0.053	2.6	3.0	0.70	97.8	2.9	0.747	7.6	131.0	10.7	0.216	**160.1**	17.6	16.5	17.1
		CSO-KHM-1 z11	2.282	2.4	3.331	1.8	0.007	16.0	0.041	3.0	3.3	0.69	87.6	2.9	0.742	7.7	118.1	10.0	0.212	**141.3**	15.3	14.7	15.0
		CSO-KHM-1 z12	1.863	2.4	2.692	1.8	0.012	14.3	0.037	3.3	3.7	0.69	98.9	3.6	0.705	8.8	140.3	13.4	0.214	**176.4**	18.7	22.0	20.3
		in_CSO-KHM-1 z12	3.332	2.4	4.509	1.8	0.014	4.8	0.058	2.7	3.1	0.74	91.5	2.8	0.719	8.4	127.3	11.5	0.228	**155.5**	16.6	19.1	17.8
		in_CSO-KHM-1 z13	1.739	2.4	2.711	1.8	0.007	4.8	0.031	3.5	3.8	0.64	83.3	3.2	0.696	9.1	119.6	11.8	0.198	**144.6**	18.2	17.9	18.0
		in_CSO-KHM-1 z5	3.852	2.4	4.999	1.8	0.015	4.8	0.068	2.3	2.8	0.77	95.2	2.6	0.772	6.9	123.4	9.1	0.238	**147.7**	16.3	16.4	16.3
		in_CSO-KHM-1 z6	6.470	2.4	5.247	1.8	0.031	4.8	0.082	2.4	2.8	1.23	100.2	2.8	0.762	7.1	131.6	10.1	0.381	**151.0**	15.3	16.6	15.9
																			Eruption age (±2σ ∗ √MSWD)[j]:	**163 (±11)**	**MSWD = 1.4**	*g.o.f.:*	*0.321*
Turnul Apor	AB	CSO-AB z1	2.259	2.4	3.141	1.8	0.003	20.0	0.110	2.4	2.8	0.72	247.8	7.0	0.744	7.7	333.0	27.2	0.199	**351.6**	31.1	34.1	32.6
		CSO-AB z2	4.816	2.4	5.845	1.8	0.010	12.3	0.220	1.9	2.4	0.82	261.3	6.3	0.773	6.8	338.0	24.4	0.228	**355.3**	29.3	29.9	29.6
		CSO-AB z3	3.825	2.4	4.969	1.8	0.011	9.6	0.174	1.9	2.4	0.77	245.9	6.0	0.779	6.6	315.6	22.3	0.213	**330.4**	24.8	27.1	26.0
																			Eruption age (±2σ ∗ √MSWD)[j]:	**344 (±33)**	**MSWD = 0.2**	*g.o.f.:*	*0.782*
Balvanyos	BAL	MK-2 z1	6.904	2.4	12.708	1.8	0.059	9.3	0.834	1.9	2.5	0.54	482.1	12.0	0.838	4.8	575.0	31.3	0.153	**578.8**	33.9	32.4	33.2
		MK-2 z2	4.601	2.4	7.137	1.8	0.032	9.8	0.430	2.0	2.5	0.64	432.8	11.0	0.793	6.2	545.5	36.5	0.181	**545.6**	40.7	34.5	37.6
		MK-2 z3	5.110	2.4	6.974	1.8	0.038	9.6	0.484	2.0	2.5	0.73	490.4	12.4	0.785	6.4	624.3	43.2	0.206	**626.7**	50.3	41.9	46.1
		MK-2 z4	4.088	2.4	7.804	1.8	0.035	9.8	0.534	2.0	2.5	0.52	504.8	12.9	0.792	6.3	637.7	43.1	0.147	**647.9**	44.7	48.9	46.8
		MK-2 z5	6.401	2.4	11.634	1.8	0.049	9.6	0.661	2.0	2.5	0.55	416.6	10.5	0.793	6.2	525.3	35.2	0.154	**524.5**	39.9	32.4	36.2
		MK-2 z6	9.839	2.4	15.556	1.8	0.111	9.4	1.066	1.9	2.5	0.63	493.7	12.2	0.828	5.2	596.1	34.1	0.178	**598.2**	39.6	33.1	36.4
		CSO-BAL(cs) z1	2.967	2.4	5.091	1.8	0.019	17.0	0.341	1.6	2.2	0.58	488.5	11.0	0.760	7.2	642.9	48.5	0.165	**646.1**	58.0	47.6	52.8
		CSO-BAL(cs) z2	3.646	2.4	5.395	1.8	0.018	17.6	0.314	1.6	2.2	0.68	416.2	9.2	0.818	5.5	509.0	30.1	0.191	**508.8**	33.5	28.6	31.0
		CSO-BAL(cs) z3	2.545	2.4	5.337	1.8	0.012	20.1	0.375	1.6	2.2	0.48	522.6	11.7	0.807	5.8	647.3	40.1	0.135	**651.6**	50.1	39.3	44.7
		CSO-BAL(cs) z4	3.998	2.4	5.685	1.8	0.030	10.9	0.372	1.6	2.2	0.70	465.1	10.2	0.783	6.5	594.0	40.8	0.199	**595.4**	46.3	39.5	42.9
		CSO-BAL(cs) z5	6.913	2.4	9.067	1.8	0.061	10.8	0.624	1.5	2.1	0.76	483.4	10.3	0.825	5.3	586.2	33.3	0.216	**587.1**	38.7	31.4	35.0
																			Eruption age (±2σ ∗ √MSWD)[j]:	**583 (±30)**	**MSWD = 1.6**	*g.o.f.:*	*0.097*
Puturosul	BH	CSO-BH z1	2.389	2.4	2.067	1.8	0.001	34.7	0.167	2.0	2.5	1.16	526.9	13.3	0.728	8.1	723.3	61.7	0.301	**741.7**	73.5	73.2	73.4

(continued on next page)

Table 4 (*continued*)

Sample name	Sample ID	Sample code	^{232}Th (ng)	± %[a]	^{238}U (ng)	± %[a]	^{147}Sm (ng)	±%[a]	^{4}He (ncc)	±%[a]	TAU[b] (%)	Th/U	Raw (U-Th)/He age (ka)	±1 s.d. (ka)	F_T[c]	±[d] (%)	F_T-cor. (U-Th)/He age[e] (ka)	±1 s.d.[f] (ka)	D_{230}[g]	Disequilibrium corrected (U-Th)/He age[h] (ka)	+1σ[i] (ka)	−1σ[i] (ka)	±1σ[i] (ka)
		CSO-BH z2	4.718	2.4	4.548	1.8	0.031	9.0	0.355	1.8	2.3	1.04	518.4	12.1	0.792	6.2	654.4	43.6	0.270	**659.7**	50.9	44.3	47.6
		CSO-BH z3	2.893	2.4	4.335	1.8	0.003	29.5	0.287	1.8	2.4	0.67	472.9	11.1	0.820	5.4	576.8	34.0	0.174	**579.9**	38.2	33.6	35.9
		CSO-BH z4	3.640	2.4	3.678	1.8	0.004	26.0	0.291	1.8	2.3	0.99	531.6	12.4	0.744	7.7	714.4	57.3	0.258	**732.8**	69.9	68.6	69.2
		CSO-BH z5[l]	3.693	2.4	5.006	1.8	0.005	17.1	0.358	1.8	2.4	0.74	504.6	11.9	0.554	13.4	911.4	123.9	0.192				
		CSO-BH z6	1.853	2.4	2.983	1.8	0.002	32.7	0.210	1.9	2.4	0.62	509.7	12.5	0.739	7.8	689.4	56.5	0.162	**699.6**	74.9	60.4	67.7
		CSO-BH(sz) z1	2.419	2.4	3.268	1.8	0.017	16.2	0.211	2.0	2.5	0.74	455.1	11.3	0.777	6.7	585.4	41.7	0.200	**586.5**	47.7	40.2	44.0
		CSO-BH(sz) z2	1.463	2.4	2.380	1.8	0.012	18.3	0.163	2.1	2.6	0.61	495.9	12.9	0.754	7.4	657.7	51.4	0.166	**663.0**	63.9	52.2	58.0
		CSO-BH(sz) z3	1.282	2.4	4.028	1.8	0.015	18.7	0.269	1.9	2.5	0.32	514.4	12.7	0.761	7.2	675.6	51.2	0.086	**686.3**	67.9	54.8	61.3
																			Eruption age (±2σ ∗ √MSWD)[j]:	**642 (±44)**	**MSWD = 1.4**	*g.o.f.:*	*0.219*
Dealul Mare	NH	CSO-NH5 z1	3.183	2.4	3.470	1.8	0.007	15.1	0.332	1.7	2.3	0.92	651.4	14.8	0.741	7.8	878.5	71.0	0.285	**885.4**	99.1	74.8	86.9
		CSO-NH5 z2	2.580	2.4	4.268	1.8	0.008	14.5	0.387	1.7	2.3	0.60	657.8	15.1	0.801	6.0	821.1	52.5	0.188	**828.4**	58.7	55.2	57.0
		CSO-NH5 z3	1.959	2.4	3.085	1.8	0.007	15.8	0.261	1.9	2.5	0.64	610.5	15.1	0.748	7.6	816.3	65.0	0.198	**820.5**	71.2	66.0	68.6
		CSO-NH5 z4	12.951	2.4	7.076	1.8	0.016	11.0	0.782	1.6	2.2	1.83	638.9	13.8	0.783	6.5	816.1	56.0	0.569	**815.1**	63.0	53.3	58.2
		CSO-NH5 z5	3.779	2.4	6.851	1.8	0.005	19.8	0.678	1.6	2.2	0.55	725.2	16.2	0.830	5.1	873.5	48.6	0.172	**888.1**	68.1	54.9	61.5
		CSO-NH5 z6	1.715	2.4	2.835	1.8	0.003	28.7	0.250	1.8	2.4	0.61	639.6	15.4	0.771	6.9	829.5	60.4	0.188	**836.4**	69.2	63.5	66.4
																			Eruption age (±2σ ∗ √MSWD)[j]:	**842 (±53)**	**MSWD = 0.2**	*g.o.f.:*	*0.927*
Bixad	MB-B	CSO-MB-B z1	3.416	2.4	5.377	1.8	0.028	12.4	0.479	1.6	2.2	0.64	641.3	14.1	0.819	5.4	783.4	45.9	0.167	**788.9**	42.2	51.6	46.9
		CSO-MB-B z2	5.790	2.4	10.203	1.8	0.066	9.4	0.982	1.4	2.1	0.57	703.0	14.9	0.835	4.9	841.9	45.3	0.150	**843.3**	47.2	46.5	46.8
		CSO-MB-B z3	7.658	2.4	9.062	1.8	0.074	11.5	1.019	1.4	2.1	0.85	776.4	15.9	0.823	5.3	943.6	53.8	0.223	**942.9**	60.3	51.2	55.8
		CSO-MB-B z4	3.463	2.4	6.325	1.8	0.028	13.7	0.617	1.5	2.1	0.55	715.2	15.3	0.807	5.8	886.8	54.9	0.144	**896.2**	49.9	64.0	57.0
		CSO-MB-B z5	3.552	2.4	4.404	1.8	0.032	12.5	0.503	1.5	2.1	0.81	793.9	16.8	0.747	7.6	1062.1	83.6	0.213	**1067.4**	98.4	87.4	92.9
		CSO-MB-B z6	3.216	2.4	5.052	1.8	0.014	18.2	0.503	1.5	2.2	0.64	717.1	15.4	0.742	7.7	966.7	77.7	0.168	**964.7**	87.3	76.1	81.7
		MB z8	2.720	2.4	4.162	1.8	0.063	24.9	0.476	1.2	2.0	0.65	821.1	16.2	0.800	6.0	1026.8	64.9	0.172	**1030.1**	72.7	65.9	69.3
		MB z9	4.309	2.4	6.814	1.8	0.165	20.0	0.756	1.1	1.9	0.63	799.2	15.2	0.799	6.0	1000.8	63.4	0.167	**1003.6**	70.3	63.6	67.0
																			Eruption age (±2σ ∗ √MSWD)[j]:	**907 (±66)**	**MSWD = 2.5**	*g.o.f.:*	*0.006*
Baba Laposa	BL	CSO-BL-1 z1[l]	23.819	2.4	15.492	1.8	0.037	6.8	1.495	1.5	2.1	1.54	585.8	12.1	0.807	5.8	726.1	44.7	0.464				
		CSO-BL-1 z2	4.143	2.4	5.630	1.8	0.007	16.8	0.603	1.6	2.2	0.74	756.1	16.7	0.805	5.9	939.5	58.8	0.222	**942.8**	66.2	58.5	62.4
		CSO-BL-1 z3	15.021	2.4	8.756	1.8	0.090	6.0	1.247	1.5	2.1	1.72	838.9	17.4	0.805	5.8	1041.9	64.6	0.517	**1047.8**	83.9	63.4	73.7
		CSO-BL-1 z4	1.797	2.4	2.769	1.8	0.002	34.3	0.293	1.9	2.4	0.65	760.0	18.3	0.773	6.8	983.4	71.1	0.196	**989.8**	94.3	74.6	84.5
		CSO-BL-1 z5	2.106	2.4	3.043	1.8	0.015	10.9	0.347	1.7	2.3	0.69	812.6	18.8	0.769	6.9	1056.5	77.1	0.209	**1101.2**	79.5	109.5	94.5
		CSO-BL-1 z6	2.637	2.4	3.527	1.8	0.002	40.1	0.379	1.7	2.3	0.75	757.4	17.1	0.774	6.8	978.9	70.0	0.225	**986.7**	85.4	75.7	80.5
		CSO-BL-1 zR2	2.813	2.4	4.046	1.8	0.041	15.9	0.417	1.8	2.4	0.70	733.2	116.9	0.777	6.7	943.4	67.0	0.210	**949.0**	73.4	71.0	72.2
		CSO-BL-1 zR4	5.016	2.4	4.437	1.8	0.034	13.8	0.425	1.9	2.4	1.13	625.7	86.1	0.800	6.0	782.1	50.5	0.341	**779.7**	55.2	47.3	51.3
		CSO-BL-1 zR5	1.147	2.4	1.885	1.8	0.007	37.6	0.202	2.0	2.5	0.61	774.4	290.9	0.740	7.8	1046.2	85.7	0.183	**1107.4**	73.7	140.4	107.1
		CSO-BL-1 zR6	1.703	2.4	1.964	1.8	0.000	0.0	0.193	2.0	3.6	0.87	674.6	0.0	0.730	8.1	924.3	82.1	0.261	**925.5**	87.3	82.6	85.0
		CSO-BL-1 zR7	4.824	2.4	6.248	1.8	0.030	21.7	0.606	1.8	2.3	0.77	679.8	147.6	0.793	6.2	857.5	57.0	0.233	**858.1**	63.2	56.9	60.1
		CSO-BL-1 zR8	4.216	2.4	4.130	1.8	0.017	24.2	0.460	1.8	2.4	1.02	743.1	179.8	0.709	8.7	1047.4	94.6	0.308	**1093.3**	89.5	139.0	114.3
																			Eruption age (±2σ ∗ √MSWD)[j]:	**942 (±65)**	**MSWD = 2.2**	*g.o.f.:*	*0.044*
Malnaş	MB-M	CSO-MB-M z4	2.687	2.4	3.082	1.8	0.016	13.6	0.355	1.2	1.9	0.87	791.3	15.3	0.754	7.4	1049.2	80.0	0.235	**1047.1**	87.0	77.5	82.3
		CSO-MB-M z5	4.460	2.4	5.782	1.8	0.053	7.5	0.651	1.3	2.0	0.77	789.3	15.7	0.816	5.5	966.9	56.6	0.208	**963.0**	63.8	52.5	58.2
		CSO-MB-M z6	2.892	2.4	3.626	1.8	0.031	9.7	0.375	1.3	2.0	0.80	719.9	14.4	0.781	6.6	921.4	63.2	0.215	**917.1**	69.9	58.5	64.2
		CSO-MB-M z7	2.318	2.4	3.603	1.8	0.013	16.5	0.387	1.3	2.0	0.64	773.0	15.5	0.777	6.7	994.8	69.5	0.174	**992.1**	76.3	65.7	71.0
		CSO-MB-M z8	7.536	2.4	9.875	1.8	0.055	8.8	1.073	1.0	1.8	0.76	762.3	14.0	0.817	5.5	933.5	54.2	0.206	**940.1**	50.7	60.9	55.8
		CSO-MB-M z9	3.426	2.4	4.902	1.8	0.034	8.1	0.505	1.2	1.9	0.70	732.2	14.2	0.781	6.6	937.6	64.3	0.189	**944.7**	60.2	71.7	65.9
		CSO-MB-M z10	3.827	2.4	5.252	1.8	0.018	14.3	0.544	1.1	1.9	0.73	732.4	13.8	0.776	6.7	944.3	66.0	0.197	**938.6**	74.2	60.3	67.3

		CSO-MB-M z11	2.612	2.4	3.319	1.8	0.014	15.0	0.380	1.2	1.9	0.79	799.7	15.5	0.773	6.8	1033.9	73.1	0.212	**1031.8**	80.3	70.6	75.4
																			Eruption age (±2σ ∗ √MSWD)[j]:	**964 (±46)**	**MSWD = 0.4**	*g.o.f.:*	*0.871*
Pilişca	PD	CSO-PD2 z4	3.253	2.4	4.660	1.8	0.027	12.4	0.802	1.4	2.1	0.70	1223.6	25.8	0.766	7.0	**1597.1**	117.0	0.216				
		CSO-PD2 z5	2.114	2.4	3.413	1.8	0.050	12.0	0.573	1.5	2.1	0.62	1213.8	26.1	0.758	7.3	**1601.5**	121.3	0.192				
		CSO-PD2 z6	4.481	2.4	4.929	1.8	0.046	9.5	0.877	1.4	2.1	0.91	1212.6	25.1	0.735	7.9	**1649.5**	135.5	0.281				
		CSO-PD2 z7	2.661	2.4	4.720	1.8	0.087	9.1	0.857	1.4	2.1	0.56	1327.4	27.8	0.782	6.5	**1696.7**	116.4	0.174				
		CSO-PD2 z8	2.040	2.4	2.551	1.8	0.032	11.4	0.436	1.5	2.1	0.80	1189.3	25.3	0.714	8.6	**1664.5**	146.9	0.247				
																Eruption age (±2σ)[k]:	**1640 (±37)**		**MSWD = 0.1**				
Murgul Mare	NM	CSO-NM1 z1	0.844	2.4	2.352	1.8	0.011	19.3	0.444	1.2	2.0	0.36	1443.1	29.2	0.777	6.7	**1856.9**	129.7	0.100				
		CSO-NM1 z2	1.666	2.4	3.818	1.8	0.013	14.5	0.787	1.1	1.9	0.44	1547.7	30.1	0.795	6.2	**1947.8**	125.9	0.121				
		CSO-NM1 z3	1.154	2.4	3.029	1.8	0.011	18.9	0.576	1.2	2.0	0.38	1444.8	28.7	0.766	7.0	**1886.6**	137.7	0.106				
		CSO-NM1 z4	2.894	2.4	7.253	1.8	0.022	13.3	1.389	1.0	1.9	0.40	1450.2	27.5	0.823	5.3	**1761.5**	99.2	0.111				
		CSO-NM1 z5	1.398	2.4	3.274	1.8	0.013	15.8	0.675	1.1	2.0	0.43	1551.4	30.3	0.750	7.5	**2068.1**	160.2	0.119				
		CSO-NM1 z6	0.814	2.4	2.056	1.8	0.009	19.4	0.373	1.3	2.0	0.40	1373.2	28.1	0.760	7.2	**1807.9**	135.5	0.110				
																Eruption age (±2σ)[k]:	**1865 (±87)**		**MSWD = 0.7**				

Note: σ = standard error, s.d. = standard deviation, MSWD = mean square of weighted deviates, g.o.f. = goodness of fit.

[a] Analytical uncertainties associated with the measurement of each isotope.

[b] TAU = total analytical uncertainty.

[c] Ft is alpha ejection correction factor calculated after Farley et al. (1996), Farley (2002) and Hourigan et al. (2005).

[d] Calculated by 30 ∗ (1 − Ft).

[e] Ft-corrected (α-ejection corrected) (U-Th)/He age.

[f] Uncertainty including analytical uncertainties and alpha ejection correction uncertainties.

[g] Zircon/magma D230 parameters were calculated using the Th/U ratios of analyzed bulk zircon crystals and whole rock (Farley et al., 2002).

[h] Disequilibrium corrected (U-Th)/He age calculated by MCHeCalc program (Schmitt et al., 2010).

[i] Uncertainty includes previous propagated errors and disequilibrium correction as calculated by MCHeCalc program (Schmitt et al., 2010).

[j] "Concordant" eruption age calculated by MCHeCalc program (Schmitt et al., 2010).

[k] Weighted mean age.

[l] Outliers omitted from the final age calculation because of their high TAU, low FT or unusually high U and Th content.

[m] Outliers omitted from the final age calculation because of the distribution test (Q-Q plot, Shapiro-Wilk test, Upton and Cook, 1996).

relative to parental ^{234}U (reasonably expected to be in equilibrium with ^{238}U). The effect of isotope disequilibrium has to be considered, however, only for Quaternary samples, because for older zircons the uncertainty related to the (U-Th)/He-method is greater than the secular disequilibrium effect on the ages (Farley et al., 2002). This correction can be performed based on the crystallization ages of analyzed zircon crystals obtained by U-Th or U-Pb zircon dating (e.g., Schmitt et al., 2006, 2010; Schmitt, 2011; Danišík et al., 2012, 2017; Lindsay et al., 2013). If crystallization ages cannot be obtained, or are heterogeneous, the "secular equilibrium assumed" (U-Th)/He age and the "full disequilibrium assumed" (U-Th)/He age will give the upper and lower age limits for the eruption age, respectively. Full disequilibrium zircon (U-Th)/He ages mean that zircon crystallized just before eruption (i.e., the zircon crystallization time is equal to the eruption age; Farley et al., 2002), whereas the "secular equilibrium assumed" (U-Th)/He age scenario applies to crystals with protracted (>375 kyr) pre-eruptive storage or to xenocrysts.

The studied samples yielded (U-Th)/He ages <2 Ma and therefore, the effects of isotope disequilibrium should be considered. For this purpose, Schmitt et al. (2006) used a combined U-Th and (U-Th)/He analysis, when the Ft-corrected (U-Th)/He data were corrected by the average crystallization age of the zircons obtained from U-Th spot interior ages. Later, Schmitt et al. (2010) refined this method and measured the U-Th and (U-Th)/He dates on the same zircon grains (double-dating). Although Danišík et al. (2017) suggested that zircon double-dating is the most accurate way to determine the eruption ages, the two methodologies provide similar result within uncertainty (e.g., Schmitt et al., 2010; Danišík et al., 2012). Schmitt et al. (2010) emphasized that in case of age-zoned crystals, the rim age provides a lower limit for the bulk crystallization age and the eruption age would be overcorrected. Zircons in the Ciomadul dacites show a wide range of crystallization age, even in single crystals (Harangi et al., 2015a), therefore, we used the weighted average U-Th (for the sample KHM) and U-Pb (for all the other samples) dates (Table 5) reported in Lukács et al. (submitted) to correct the initial Th disequilibrium. The corrected ages were computed using the MCHeCalc software (http://sims.ess.ucla.edu/Research/MCHeCalc.php) following the description provided by Schmitt et al. (2010). However, in case of the youngest sample (KHM) both double-dating and average crystallization age correction were applied (1) to perform accurate eruption age with the standard technique (Schmitt et al., 2006, 2010) and (2) to monitor the effect of different corrections on the accuracy of the final date. Zircon/magma D_{230} parameters (Farley et al., 2002) were calculated using the Th/U ratios of analyzed bulk zircon crystals and whole rock (Table 4). We assumed secular equilibrium for ^{231}Pa (i.e. $D_{231} = 1$) because the ^{4}He contribution from the ^{235}U decay series is minor, and the effects of disequilibrium are negligible within reasonable limits of D_{231} (Schmitt, 2011). The results of these calculations are presented in Table 4, Appendix 2 and Fig. 4. Uncertainties were calculated by multiplying the 2-sigma error with the square root of the MSWD (e.g., Danišík et al., 2012).

The "full disequilibrium assumed" (U-Th)/He time yields the maximum possible eruption age for every sample, assuming no zircon residence time (Appendix 2). However, it is very useful also for identifying the outlier dates and indicating the necessity of the Th-disequilibrium correction (i.e., if the "secular equilibrium assumed" and the "full disequilibrium assumed" ages are overlapping with each other, no Th-disequilibrium correction is needed). The two oldest CAs-samples yielded (U-Th)/He weighted mean ages of 1954 ± 48 ka (Murgul Mare; NM) and 1696 ± 22 ka (Pilişca; PD) for "full disequilibrium assumed", which are indistinguishable within uncertainties from the disequilibrium-uncorrected He ages (1865 ± 87 ka and 1640 ± 37 ka, respectively). Therefore, no disequilibrium correction is required for these samples and the "secular equilibrium assumed" (U-Th)/He ages approximate well the eruption ages. For all the other samples with ages <1.5 Ma, the "full disequilibrium assumed" (U-Th)/He ages (Appendix 2) differ from the "secular equilibrium assumed" (U-Th)/He ages, thus a disequilibrium correction is applied (Table 4). The correction significantly increases zircon dates for samples <500 ka, whereas the U-Pb corrected (U-Th)/He ages for samples with ages between ca. 1 Ma and 500 ka shifted only slightly because of the large (i.e., ~100 kyr) average zircon residence time during which zircon largely attained secular equilibrium prior to eruption.

A direct comparison of the double-dating method (Schmitt et al., 2010; Danišík et al., 2012, 2017), and the average crystallization age method (Schmitt et al., 2006; Danišík et al., 2012; Harangi et al., 2015a) was carried out for sample KHM (Table 6). The combined U-Th and (U-Th)/He double-dating results are 154 ± 16 ka ($n = 4$, goodness of fit: 0.952), which is slightly younger but overlaps within uncertainty with the average crystallization age corrected (U-Th)/He age (i.e., 163 ± 11 ka; Fig. 5). Both calculated eruption ages are consistent with the youngest rim age of the zircon grains (142 ± 18 ka; Table 5; Lukács et al., submitted), which gives a maximum age limit for the eruptions (Fig. 4).

Table 5
The average U-Pb and U-Th crystallization ages of the studied samples calculated from data presented by Lukács et al. (submitted).

Sample name	Sample ID	Method	Number of data (used/all)	Weighted mean age [ka]	Uncertainty (2σ; LA-ICP-MS and 1σ**; SIMS) [ka]	MSWD	Youngest spot age [ka]	Uncertainty (2σ; LA-ICP-MS and 1σ**; SIMS) [ka]
Haramul Mic	CSO-KHM1 SIMS mantle[a]	U-Th	24/25	198	15**	2.3	154	14**
	CSO-KHM1 SIMS rim	U-Th	21/21	179	11**	1.1	142	18**
Turnul Apor	CSO-AB LA-ICP-MS mantle[a]	U-Pb	33/49	471	35	28	395	29
	CSO-AB SIMS rim		20/20	365	47**	0.37	304	96**
Balvanyos	MK2 SIMS mantle[a]		18	864	68**	1.6	608	99**
	CSO-BAL(cs) SIMS rim		20/20	731	60**	2.1	577	74**
	CSO-BAL03 LA-ICP-MS rim		20/20	803	58	6.4	658	80
Puturosul	CSO-BH LA-ICP-MS mantle[a]		20/23	841	47	19	730	46
	CSO-BH SIMS rim		5/5	715	87**	2.1	650	91**
Dealul Mare	CSO-NH5[a]		40/44	1004	33	11.2	864	60
Bixad	CSO-MB-B[a]		33/38	1226	38	10.8	1075	62
Baba-Laposa	CSO-BL1[a]		38/44	1129	34	8.3	980	72
Malnaş	CSO-MB-M[a]		38/43	1332	47	25	1140	92
Pilişca	CSO-PD2		40/45	1867	42	1.3	1708	85
Murgul Mare	CSO-NM1		47/60	2165	45	9.3	1940	95

[a] Average U-Th and U-Pb crystallization ages which were used for the disequilibrium correction in MCHeCalc program.

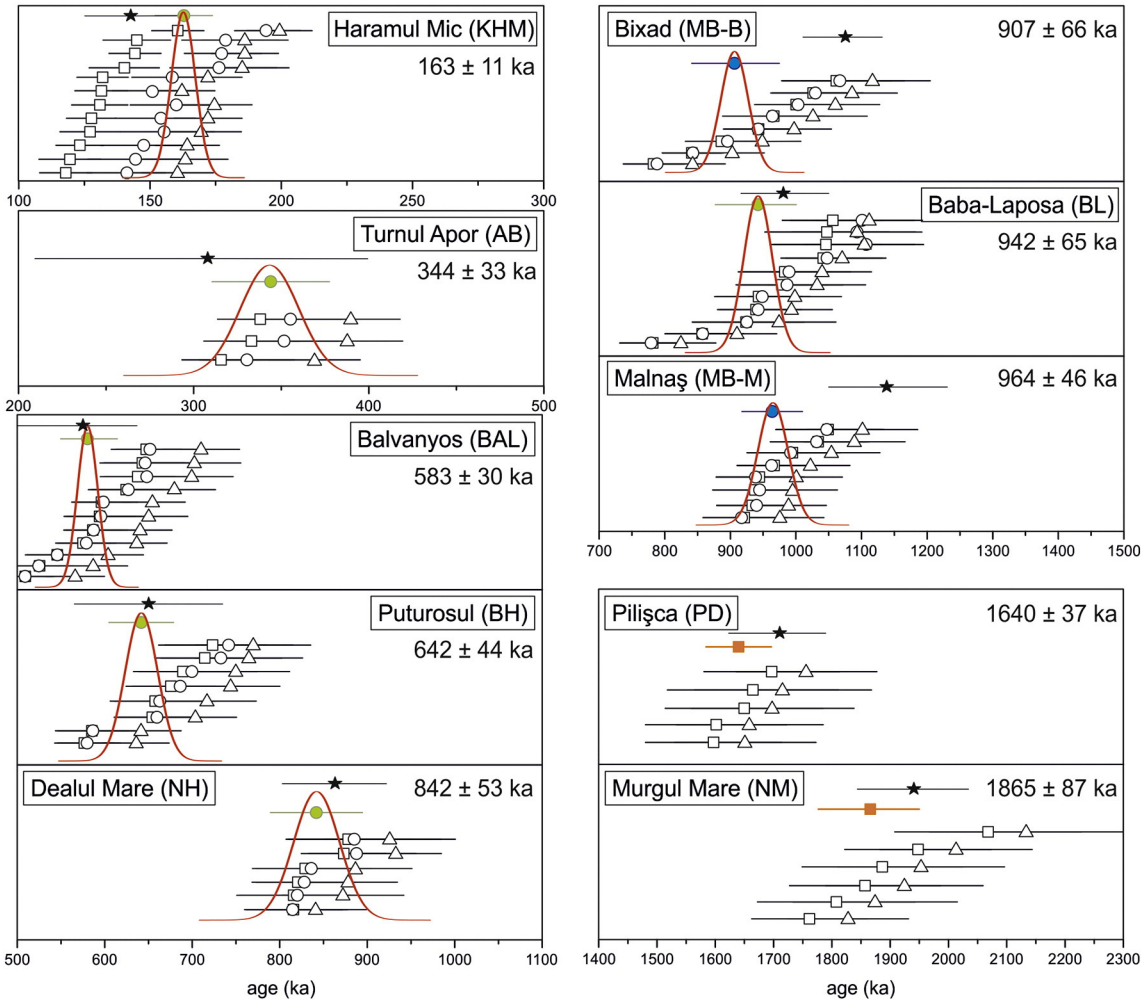

Fig. 4. Combined U-Th-Pb and (U-Th)/He zircon ages. Each panel shows the "secular equilibrium-assumed" (rectangle), the disequilibrium-corrected (circle) and "full disequilibrium-assumed" (triangle) (U-Th)/He ages, the weighted means of the disequilibrium corrected ages (filled circle/rectangle), a Gaussian fit to replicate analyses representing the modeled "concordant" eruption ages (red Gaussian curve) and the youngest crystallization ages (filled star) with uncertainties. The obtained eruption ages with $2\sigma * \sqrt{MSWD}$ uncertainties are indicated in every panel for each sample. Color coding of panels/samples see Fig. 2.

5. Discussion

5.1. Eruption chronology

The Ciomadul Volcanic Dome Complex is the youngest manifestation of the Neogene to Quaternary volcanism of the entire Carpathian-Pannonian region. Harangi et al. (2015a) determined the eruption ages of the youngest volcanic phase of the Ciomadul volcano using the same methodology as in this study. The eruption ages derived from the zircon (U-Th)/He dates corrected for disequilibrium correspond to 56 to 32 ka. This dominantly explosive volcanic episode was preceded by an effusive phase with prevailing lava dome extrusions, where the uncorrected zircon (U-Th)/He dates presented in Karátson et al. (2013) indicate eruption ages between ca. 200 and 100 ka. Here, the

Table 6
Dataset of measurements and corrections of the double dated KHM sample. For the detailed dataset of the (U-Th)/He analysis and the footnotes please refer to Table 4.

Sample name	Sample ID	Sample code	$(^{238}U)/(^{232}Th)$	±	$(^{230}Th)/(^{232}Th)$	±	F_T-cor. (U-Th)/He age[e] (ka)	±1 s.d.[f] (ka)	D^g_{230}	U-Th age (ka)	+ (ka)	− (ka)	Disequilibrium corrected (U-Th)/He age[h] (ka)	$+1\sigma^i$ (ka)	$-1\sigma^i$ (ka)	$\pm1\sigma^i$ (ka)
Haramul Mic	KHM	in_CSO-KHM-1 z12	8.44	0.2	6.73	0.2	127.3	11.5	0.228	162	19	16	**155.5**	16.6	19.1	17.8
		in_CSO-KHM-1 z13	8.41	0.2	7.26	0.2	119.6	11.8	0.198	172	22	23	**144.6**	18.2	17.9	18.0
		in_CSO-KHM-1 z5	6.52	0.2	5.44	0.2	123.4	9.1	0.238	181	29	23	**147.7**	16.3	16.4	16.3
		in_CSO-KHM-1 z6	3.44	0.1	2.95	0.1	131.6	10.1	0.381	180	36	27	**151.0**	15.3	16.6	15.9
											Eruption age (±2σ)[j]:		**154 (±16)**		*g.o.f.:*	*0.952*

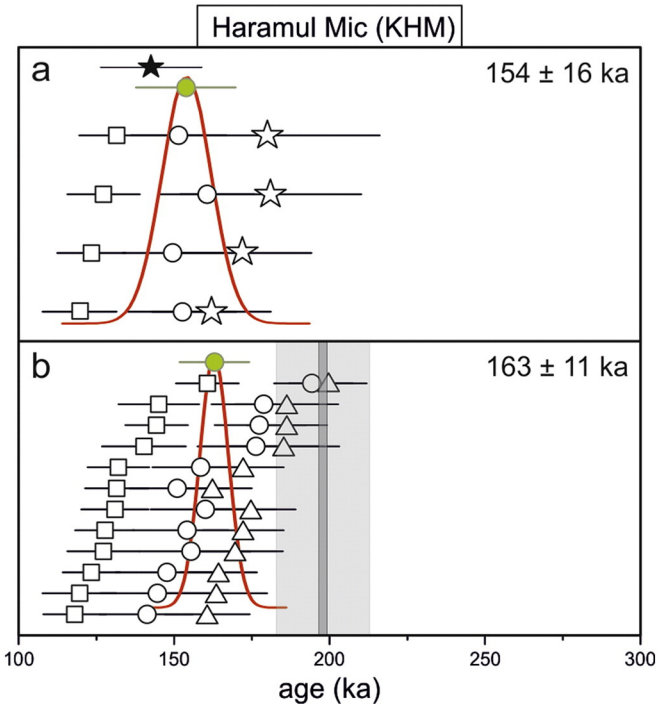

Fig. 5. Comparison between the double-dating (a) and the average crystallization age correction (b) method. Uncertainties for the obtained ages are 2σ for the double-dating approach (a) and 2σ ∗ √MSWD for the average crystallization age correction (b). U-Th ages of the dated zircon grains (star), youngest crystallization age (filled star) and average crystallization age (grey bar) with uncertainties are indicated, further symbols and colors as in Fig. 4.

eruption chronology is extended to the initial stage of CVDC volcanism, when multiple isolated, mainly dacitic lava domes were formed. We dated all identified localities, where K/Ar ages were already determined (Table 1.), but additionally the Turnul Apor lava was also sampled which has not been dated yet. This complete eruption age coverage for the early CVDC yields a precise age framework on the repose time between eruptions.

Eruption ages inferred from (U-Th)/He zircon cooling ages (Table 4, Appendix 2) for the peripheral CVDC lava domes are in the range between 964 and 580 ka (the 344 ka Turnul Apor is not in a peripheral position), whereas the Haramul Mic lava dome was erupted at 154 ± 16 ka. These ages, which are supported also by the youngest zircon crystallization ages (Table 5; Lukács et al., submitted) are much younger than the previously determined K/Ar ages (Pécskay et al., 1992, 1995; Szakács et al., 2015; Table 1). The most pronounced difference is found between the K/Ar age and zircon (U-Th)/He age of the Haramul Mic dacite (850 ka in Casta (1980), while 154 ka in this study) and the Malnaş-Bixad shoshonites (2.2–1.4 Ma in Peltz et al. (1987), while 964–907 ka in this study). Because most of the studied sites (excluding the Pilişca volcanic complex) represent small-volume lava domes (~0.1–0.6 km^3 based on DEM analysis; Szakács et al., 2015), they likely formed monogenetically during a short period of time. Evidence for eruptive hiatuses is absent, and it is thus unlikely that the differences between K/Ar and (U-Th)/He dates are due to age heterogeneity within individual domes. Instead, it is conceivable that K/Ar dates are affected by unidentified excess argon, and therefore yield apparent older ages (e.g., Hora et al., 2007; Hildenbrand et al., 2012). The contribution of excess ^{40}Ar is potentially aggravated by the abundance of porphyritic rocks in the CVDC, where mineral phases crystallized during open-system magmatic processes over a prolonged period in a crustal magma reservoir (Kiss et al., 2014; Harangi et al., 2015a, 2015b). The unknown effect of excess argon during K/Ar dating makes zircon-based geochronology – in this case (U-Th)/He dating – more reliable and robust. Furthermore, the concordant ages of radiocarbon, thermoluminescence, and (U-Th)/He zircon ages for the same eruptive products of the youngest volcanic rocks of the Ciomadul volcano (Harangi et al., 2015a) validate the applicability and accuracy of the (U-Th)/He zircon geochronology on these young volcanic rocks.

Palaeomagnetic data of Panaiotu et al. (2012) serve as an independent control for the proposed eruption ages. Our new combined U-Th-Pb and (U-Th)/He zircon ages are in good agreement with published palaeomagnetic polarity data (Fig. 6). Specifically, normally magnetized Malnaş could correspond to the short-lived Santa Rosa excursion, which is possibly also the case for Bixad, although eruption during the Kamikatsura excursion (Singer, 2014) is also conceivable within analytical uncertainties. The normally magnetized Balvanyos and the reversed Pilişca correspond to the Bruhens and Matuyama chrons, respectively. The eruption age of Murgul Mare which has a transitional magnetic character (Panaiotu et al., 2012) correlates well with the Olduvai excursion.

This new, detailed dating of the eruption products of the older phase of the CVDC enables to reconstruct the following eruption history for the South Harghita over the past 2 Myr (Fig. 7). The oldest two samples are the 1865 ± 87 ka andesitic lava dome of Murgul Mare and the younger, 1640 ± 37 ka dacitic part of the Pilişca volcano, which predate well the activity of the CVDC (Fig. 7A). Further eruptions during this period cannot be excluded, although, the PD dacite is inferred to be one of the youngest volcanic product at Pilişca (Szakács et al., 2015). In this case, a ca. 600 kyr quiescence period preceded the initial CVDC volcanism. Within a relatively short period (<100 kyr), three lava domes were formed: two HKS lava bodies (Malnaş: 964 ± 46 ka; and Bixad: 907 ± 66 ka) in the vicinity to the site of the Murgul Mare and the first HKCA lava dome of Baba-Laposa (942 ± 65 ka), which emerged at the foot of the Pilişca volcano. In particular, extrusion of the Baba-Laposa dacite with the unique chemical composition, which is indistinguishable from the later CVDC dacites could be a sign of the onset of the development of the CVDC. These three lava domes are arranged parallel to the river Olt (Fig. 7B). This alignment corresponds to a NNE-SSW trending normal fault system, which follows the orientation of the main normal faults of the Braşov (and Ciuc) basin (Girbacea et al., 1998; Ciulavu et al., 2000; Seghedi et al., 2011) and is perpendicular (i.e., NNE-SSW) to the NW-SE orientation of the CGH volcanic chain.

After a short (<100 kyr) repose time, an andesitic HKCA lava dome (Dealul Mare: 842 ± 53 ka) was formed which was followed by two adjacent dacitic lava domes (Puturosul: 642 ± 44 ka and Balvanyos: 583 ± 30 ka; Fig. 7B) after ca. 100 kyr quiescence. After another, ca. 100 kyr dormancy the Turnul Apor dacitic lava (344 ± 33 ka) erupted. The four lava domes of Dealul Mare, Puturosul, Balvanyos and Turnul Apor are situated on the eastern side of the river Olt and their positions follow the NW-SE orientation of the CGH volcanic chain. The central lava dome complex of the Ciomadul volcano is located perpendicular to the NW-SE orientation of the CGH volcanic chain and shows a similar elongation as the NNE-SSW aligned ca. 1000–900 ka Malnaş, Bixad and Baba-Laposa lava domes. The onset of volcanism at the more voluminous (~8–9 km^3; based on DEM analysis Szakács et al., 2015) Ciomadul volcano occurred <200 ka (based on the uncorrected He ages of the oldest lava dome rocks presented in Karátson et al., 2013), i.e., after another protracted (>100 kyr) quiescence period. The Haramul Mic lava dome is separated from the main massif of the volcano, but its age (154 ± 16 ka) clearly suggests that it belongs to the lava dome building phase of Ciomadul volcano (Fig. 7C). A prolonged quiescence period repeats between the Ciomadul lava dome extrusion phase and the more dominant explosive volcanic phase between around 100 and 60 ka.

In summary, long repose times between eruptions characterize the volcanism of the CVDC. Such long quiescence between eruption phases is not uncommon in volcanoes fed by intermediate magmas (e.g., Lassen Peak, USA, Clynne and Muffler, 2010; Aucanquilcha, Andes, Chile;

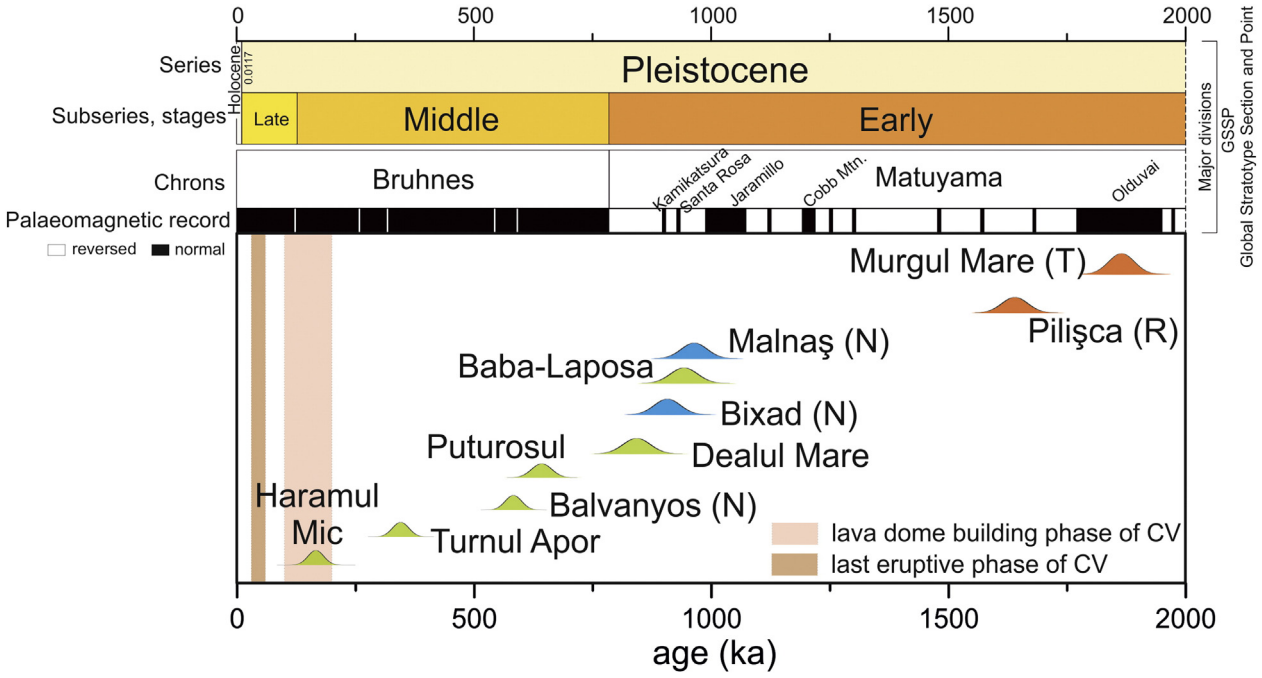

Fig. 6. Temporal evolution of the studied samples supplemented with uncorrected He ages published in Karátson et al. (2013), combined U-Th and (U-Th)/He ages from Harangi et al. (2015a) and the available polarity information (indicated by (N: normal), (R: reversed) or (T: transitional)) from Panaiotu et al. (2012). Geomagnetic Polarity Time Scale is after Singer (2014). CV: Ciomadul volcano. Color coding of samples as in Fig. 2.

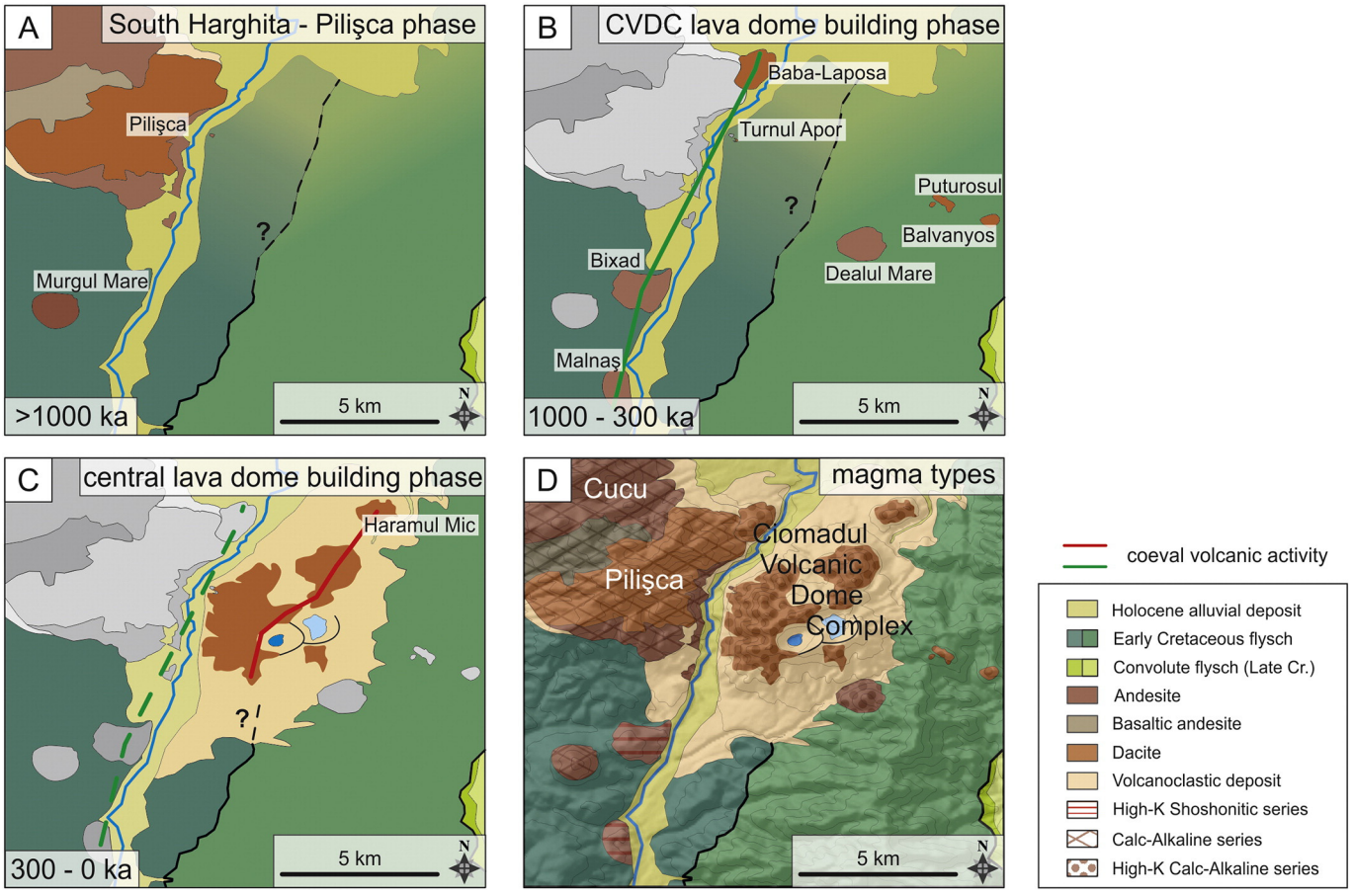

Fig. 7. A–C: Volcanological evolution of the South Harghita in the past 2 million years based on the eruption ages calculated from zircon (U-Th)/He dates (Harangi et al., 2015a; this study) and the disequilibrium uncorrected He dates of the oldest lava dome rocks of the Ciomadul volcano (Karátson et al., 2013). Green and red lines indicate the coeval volcanic activity at ca. 1 Ma and 150–100 ka, respectively. The eruption centers in these two time intervals (B and C) are arranged perpendicular to the normal, NW-SE trend of the CGH. D: Magma type distributions of the Southernmost Harghita.

Klemetti and Grunder, 2008; Sabalan, Iran, Ghalamghash et al., 2016; Ruapehu, New Zealand, Gamble et al., 2003; among others). The seemingly inactive state, however, does not indicate that the magmatic system beneath the volcano is inactive. Harangi et al. (2015a) showed that zircon crystallization ages are in the range from ca. 350 ka to 80 ka in the youngest volcanic products of Ciomadul suggesting a prolonged presence of melt-bearing magma. This implies that the comparatively brief ca. 32 kyr quiescence after the most recent CVDC eruption alone is not necessarily indicative for the magmatic system being already extinct. Multiple lines of evidence (Vaselli et al., 2002; Popa et al., 2012; Kiss et al., 2014; Harangi et al., 2015a, 2015b; Kis et al., 2017) suggests continued presence of a melt-bearing magma body beneath Ciomadul with a potential for rapid rejuvenation of this crystal mush. This led Harangi et al. (2015a, 2015b) to introduce a new term for such long-period repose volcanoes: volcanoes with Potentially Active Magma Storage (PAMS volcanoes).

5.2. Relations between magma type and eruption age

The determined eruption ages along with the bulk rock composition of the dated volcanic products enable to delineate the changes in the erupted magma composition. The first major change in magma type occurred after the time gap at 3.9–2.8 Ma within the South Harghita that divides the Luci-Lazu volcanic complex (4.3–3.6 Ma; Pécskay et al., 1995) from the volcanoes located southward (i.e., Cucu, Pilişca and Ciomadul). The erupted magmas became more potassic and show a different trace element signature than the older rocks to the north (Seghedi et al., 1987; Szakács et al., 1993; Mason et al., 1996; Harangi and Lenkey, 2007; Harangi et al., 2007; Vinkler et al., 2007). This change was interpreted as the result from (1) the tectonic inversion in the East Carpathians recorded at the beginning of the Quaternary and (2) the change in the collision mechanism caused by the difference in rheology of the continental blocks, i.e., the East European Plate and the Moesian Plate north and south from the Trotuş fault (Cloetingh et al., 2004; Harangi and Lenkey, 2007; Seghedi et al., 2011). Although, the post-2.8 Ma rocks have a more potassic character, the Cucu (2.8–2.2 Ma; Pécskay et al., 1995), Pilişca (2.6–1.5 Ma; Pécskay et al., 1995) and Murgul Mare volcanic rocks resemble the normal calc-alkaline series of the CGH rather than the youngest CVDC, which comprises HKCAs volcanic products. Thus, another major change in the composition of the erupted magmas occurred at 1 Ma, when the first HKCAs dacite and HKSs shoshonitic rocks erupted. The dominantly dacitic lava domes of the CVDC have a more pronounced Sr and Ba enrichment and depletion in the heavy REE (Seghedi et al., 1987; Szakács et al., 1993; Mason et al., 1996; Vinkler et al., 2007), although they are compositionally heterogeneous. The lava domes of Malnaş and Bixad are distinct compared to the monotonous HKCAs dacites of the CVDC. Although the change in the magma composition around 1–1.6 Ma has been previously inferred (e.g., Seghedi et al., 2011), our new combined geochronological and geochemical data provide more accurate constrains on it.

The position of the Baba-Laposa lava dome has been debated: it has been attributed to either Pilişca volcano (e.g., Szakács et al., 2015) or to Ciomadul (e.g., Seghedi et al., 1987). Here, we propose that it represents the oldest member of the CVDC. The HKSs shoshonitic magmas were previously considered to have erupted within or before the 1.6–1.0 Ma eruptive hiatus (e.g., Seghedi et al., 2011; Panaiotu et al., 2012; Szakács et al., 2015). Our new data indicate that they extruded much later, at 1000–900 ka. Remarkably, during a short period (i.e., within a few 10s kyr), eruptions of three different magma types (HKCAs and two distinct HKSs ones; Figs. 2 and 7B) occurred within a restricted area, a few km from one another. These volcanic products are distinct in chemical composition, but they have roughly similar mineral assemblage and textural features, showing evidence for open-system processes, i.e., mixing of distinct magmas (Mason et al., 1995, 1996). After a short time (a few 10s kyr), another viscous, crystal-rich magma batch with andesitic bulk composition extruded forming the Dealul Mare lava dome. Although it is less silicic than the dominant HKCAs rocks of Ciomadul, it shows a clear geochemical and petrologic affinity to them indicating possibly more mafic magma component. After the eruption of the 842 ka Dealul Mare andesite, there has been no major change in the composition of the erupted magmas: they comprise homogeneous HKCAs dacite which built up the more voluminous Ciomadul volcano. The compositional and textural variations of phenocrysts reflect still open-system magma genesis involving both mafic and silicic magmas (Kiss et al., 2014).

6. Conclusions

1. The newly determined eruption ages enable us to constrain the onset of volcanism in the Ciomadul Volcanic Dome Complex, the youngest volcanic area of eastern-central Europe. The eruption chronology has been significantly refined, revealing that many eruptions are younger than previously thought based on K/Ar data. The CVDC volcanism started at ca. 1 Ma after several 100s kyr of quiescence and was characterized by intermittent lava dome extrusions until 344 ka. This was followed by the development of the voluminous Ciomadul volcano from about 170 to 32 ka after another prolonged repose time.
2. In the South Harghita region, at least three major erupted magma types can be distinguished. A sharp change in the erupted magma composition is recognized at ca. 1 Ma following an earlier compositional shift at 2.8 Ma as defined by Pécskay et al. (2006). Initially, distinct high-K magma types erupted in the CVDC within a short (a few 10s kyr) period and in a spatially restricted area. However, since 650 ka, volcanism is characterized by eruption of homogeneous dacitic magma.
3. Dating the volcanic activity of all identified eruptive CVDC centers, predating the development of the Ciomadul volcano, allowed us to constrain the repose intervals between eruption events. It is pointed out that the volcanic eruptions were often separated by prolonged, i.e., >100 kyr quiescence periods. Recurrence of volcanism even after such long episodes of dormancy has to be considered in assessing volcanic hazards, particularly in seemingly inactive volcanic areas, where no Holocene eruptions have occurred. The proposed term of “volcanoes with Potentially Active Magma Storage” (Harangi et al., 2015a, 2015b) emphasizes the potential of volcanic rejuvenation in such volcanic regions.

Acknowledgements

This research was financed by the Hungarian National Research, Development and Innovation Fund (NKFIH) within No. K116528 and No. PD 121048 projects. The GATAN MiniCL facility belongs to the KMP project nr. 4.2.1/B-10-2011-0002 supported by the European Union. Kata Molnár was subsidized by the Talented Student Program of the Eötvös Loránd University (Budapest, Hungary) and by the Campus Hungary Short Term Study Program (Balassi Institute (B1/1R/14869), Hungary). I. Seghedi benefited by a grant of the Ministry of Education and Scientific Research, CNCS-UEFISCFI, project number PN-II-IDPCE-2012-4-0137. The HIP facility at Heidelberg University is operated under the auspices of the DFG Scientific Instrumentation and Information Technology programme. The invaluable help of Judit Dunklné Nagy (Göttingen) during the (U-Th)/He measurements is very much appreciated. The authors thank the members of the MTA-ELTE Volcanological Research Group (Budapest) for their helps during the field and laboratory works.

Appendix 1. Bulk rock composition of the studied southernmost Harghita samples

sample code in the text	PD	BL	BH		BAL		NH		MB-B	MB-M	NM		KHM		AB
	CSO-PD2	CSO-BL1	BH	CSO-BH2	CSO-BAL	CSO-BAL (cs)	CSO-NH2	CSO-NH3	CSO-MB1	CSO-MB-M	CSO-NM1	CSO-NM2	CSO-KHM1C	CSO-KHM2A3	CSO-AB1
SiO_2	66.61	63.23	64.80	63.23	64.61	63.12	59.4	58.5	58.5	57.8	61.8	61.9	65.9	65.7	64.9
TiO_2	0.56	0.45	0.53	0.54	0.53	0.52	0.7	0.8	0.9	0.9	0.7	0.7	0.4	0.3	0.4
Al_2O_3	17.64	17.26	17.30	17.81	17.77	17.50	18.1	18.4	15.5	16.3	18.3	17.7	16.1	16.2	16.9
Fe_2O_3	2.37	3.99	2.83	3.33	2.87	4.04	4.7	4.9	5.3	5.3	5.0	4.9	3.5	3.3	3.9
MnO	0.02	0.08	0.05	0.05	0.05	0.08	0.1	0.1	0.1	0.1	0.1	0.1	0.1	0.1	0.1
MgO	0.47	1.57	1.80	1.64	1.90	2.18	2.8	3.0	4.6	4.6	2.4	2.2	1.5	1.5	1.6
CaO	2.94	4.50	4.07	3.91	4.43	4.72	5.5	5.8	7.0	7.3	5.2	5.8	3.6	3.4	3.8
Na_2O	3.87	4.06	4.48	4.26	4.51	4.51	4.1	4.1	3.6	3.9	4.0	4.2	4.1	4.1	4.4
K_2O	2.70	3.22	3.27	3.27	3.29	3.15	2.6	2.6	4.0	3.5	2.4	2.4	3.4	3.2	3.2
P_2O_5	0.15	0.16	0.10	0.16	0.14	0.17	0.2	0.2	0.5	0.3	0.2	0.2	0.1	0.1	0.2
Cr	14	14	110	21	131		103	21	145	164	34	27	27	27	34
Ni	<20	<20	<20	<20	<20	<20	<20	<20	45	32	<20	<20	<20	<20	<20
Sc	8	7	8	8	8	8	12	13	13	16	14	13	5	5	6
Ba	1284	1429	1472	1509	1493	1534	1164	1215	2707	1454	948	847	1283	1306	1506
Be	3	2	2	3	3	2	2	<1	2	3	2	1	2	3	3
Co	4.4	5.7	5.9	6.1	6.6	8.0	8.7	9.2	15.5	21.9	12.4	10.7	5.9	6	7
Cs	12.4	4.5	3.3	3.7	3.8	2.1	2.8	3.0	1.6	0.8	2.1	1.9	4.2	4	13
Ga	16.0	18.3	19.3	18.1	18.5	19.2	18.2	19.4	18.1	18.5	17.6	17.3	17.3	17	18
Hf	3.1	3.6	3.9	3.7	3.6	3.4	3.3	3.5	6.6	4.8	3.7	3.5	4.0	4	4
Nb	17.1	14.8	15.5	16.5	13.9	14.4	15.5	15.4	17.6	18.9	19.7	18.0	13.4	13	15
Rb	87.2	83.4	82.4	85.6	81.7	71.4	58.2	58.3	69.0	58.2	73.9	72.8	95.6	96	86
Sn	1	1	2	1	2	<1	2	2	1	1	1	<1	2	<1	1
Sr	844.8	1209.3	1316.4	1264.5	1281.5	1354.2	1167.4	1248.6	2509.5	1713.7	696.8	732.1	1221.1	1213	1416
Ta	1.2	1.0	0.8	1.1	0.9	0.8	1.0	1.0	1.1	1.1	1.5	1.3	1.0	1	1
Th	12.6	13.6	11.9	12.2	11.4	11.3	9.0	9.7	14.8	10.0	10.8	9.5	14.9	14	14
U	3.9	4.1	3.1	3.3	3.2	3.2	2.8	2.7	3.9	2.7	3.0	3.0	4.6	5	4
V	76	61	61	75	64	64	101	112	108	117	79	94	45	46	46
W	1.2	1.1	0.9	0.7	0.9	0.5	1.4	0.7	1.1	2.8	1.2	3.2	1.5	1	2
Zr	126.3	134.9	145.9	148.9	141.9	137.1	127.5	133.5	255.0	197.9	146.8	139.1	148.1	145	158
Y	27.8	12.3	10.1	11.3	11.0	11.8	12.0	13.0	16.2	14.8	14.0	15.8	9.1	10	10
La	47.9	35.1	36.8	41.4	39.0	38.1	30.2	31.3	108.0	49.9	31.9	27.8	33.9	33	43
Ce	86.9	63.2	59.8	65.8	67.0	66.2	52.7	59.0	199.8	96.2	51.9	44.9	57.5	56	71
Pr	8.94	6.15	5.84	6.24	6.81	6.66	5.51	5.72	22.21	10.68	5.16	4.83	5.67	5	6
Nd	34.70	22.50	19.20	21.80	23.50	22.60	21.00	21.70	82.90	39.60	18.30	17.70	20.40	19	21
Sm	6.84	3.32	3.02	3.43	3.42	3.40	3.25	3.51	10.89	5.76	2.82	3.06	2.94	3	3
Eu	2.19	0.96	0.94	1.04	1.03	1.03	1.08	1.08	2.73	1.53	0.86	0.97	0.91	1	1
Gd	6.77	2.74	2.28	2.59	2.65	2.86	2.93	3.05	6.85	4.06	2.73	2.98	2.40	2	2
Tb	1.02	0.38	0.31	0.35	0.37	0.35	0.39	0.46	0.75	0.49	0.42	0.46	0.31	0	0
Dy	5.84	2.13	1.61	1.87	2.09	1.97	2.18	2.18	3.74	2.61	2.42	2.88	1.79	2	2
Ho	1.24	0.44	0.33	0.38	0.38	0.41	0.43	0.47	0.57	0.49	0.47	0.56	0.34	0	0
Er	3.28	1.17	0.98	1.18	1.26	1.17	1.25	1.26	1.49	1.39	1.50	1.69	1.00	1	1
Tm	0.52	0.21	0.15	0.20	0.16	0.18	0.19	0.18	0.25	0.20	0.22	0.25	0.16	0	0
Yb	3.34	1.44	1.13	1.26	1.08	1.18	1.15	1.23	1.47	1.36	1.41	1.65	1.12	1	1
Lu	0.49	0.22	0.17	0.21	0.19	0.20	0.20	0.22	0.22	0.19	0.25	0.27	0.16	0	0
LOI	2.7	1.5	0.8	1.8	-0.1	0.3	1.9	1.8	0.0	0.8	1.5	1.1	1.5	2.0	0.8

Appendix 2. "Secular equilibrium-assumed"-, combined U-Pb/U-Th- and "full disequilibrium-assumed" (U-Th)/He ages of the studied samples with their 1σ uncertainties, weighted means and D230 values used for the calculation

	Secular eq. assumed (U-Th)/He	1σ	D230	Combined U-Pb / U-Th and (U-Th)/He	+1s	−1s	Full diseq. assumed (U-Th)/He	1σ
KHM: 163 ± 11 (0.321)								
CSO-KHM-1 z1	145.1	12.9	0.26	**178.9**	16.7	20.2	186.2	16.5
CSO-KHM-1 z2	127.8	9.5	0.20	**154.3**	17.6	13.1	172.2	12.9
CSO-KHM-1 z3	132.1	9.8	0.26	**158.6**	15.4	14.8	172.2	12.9
CSO-KHM-1 z5	144.4	9.9	0.25	**177.4**	14.2	15.2	186.2	12.8
CSO-KHM-1 z6	160.7	10.0	0.31	**194.3**	12.0	13.2	199.4	12.4
CSO-KHM1 z10	131.0	10.7	0.22	**160.1**	17.6	16.5	174.7	14.3
CSO-KHM1 z11	118.1	10.0	0.21	**141.3**	15.3	14.7	160.6	13.6
CSO-KHM1 z12	140.3	13.4	0.21	**176.4**	18.7	22.0	185.2	17.8
in_CSO-KHM-1 z12	127.3	11.5	0.23	**155.5**	16.6	19.1	169.6	15.3
in_CSO-KHM-1 z13	119.6	11.8	0.20	**144.6**	18.2	17.9	163.6	16.2
in_CSO-KHM-1 z5	123.4	9.1	0.24	**147.7**	16.3	16.4	164.3	12.2
in_CSO-KHM-1 z6	131.6	10.1	0.38	**151.0**	15.3	16.6	162.3	12.5
Weighted means:	**133.1**	3.5					174.7	4.6

(continued on next page)

(*continued*)

	Secular eq. assumed (U-Th)/He	1σ	D230	Combined U-Pb / U-Th and (U-Th)/He	+1s	−1s	Full diseq. assumed (U-Th)/He	1σ
AB: 344 ± 33 ka (0.782)								
CSO-AB z1	333.0	27.2	0.20	**351.6**	31.1	34.1	387.7	31.7
CSO-AB z2	338.0	24.4	0.23	**355.3**	29.3	29.9	389.7	28.2
CSO-AB z3	315.6	22.3	0.21	**330.4**	24.8	27.1	369.0	26.1
Weighted means:	**327.7**	14.1					382.1	6.6
BAL: 583 ± 30 ka (0.097)								
MK-2 z1	575.0	31.3	0.15	**578.8**	33.9	32.4	636.4	34.8
MK-2 z2	545.5	36.5	0.18	**545.6**	40.7	34.5	603.6	40.5
MK-2 z3	624.3	43.2	0.21	**626.7**	50.3	41.9	679.4	47.1
MK-2 z4	637.7	43.1	0.15	**647.9**	44.7	48.9	699.2	47.3
MK-2 z5	525.3	35.2	0.15	**524.5**	39.9	32.4	586.6	39.4
MK-2 z6	596.1	34.1	*0.18*	**598.2**	39.6	33.1	654.3	37.5
CSO-BAL(cs) z1	642.9	48.5	0.17	**646.1**	58.0	47.6	702.2	53.1
CSO-BAL(cs) z2	509.0	30.1	0.19	**508.8**	33.5	28.6	566.0	33.5
CSO-BAL(cs) z3	647.3	40.1	0.14	**651.6**	50.1	39.3	709.9	44.1
CSO-BAL(cs) z4	594.0	40.8	*0.20*	**595.4**	46.3	39.5	650.1	44.7
CSO-BAL(cs) z5	586.2	33.3	0.22	**587.1**	38.7	31.4	640.3	36.5
Weighted means:	**579.7**	18.4					648.0	14.5
BH: 642 ± 44 ka (0.219)								
CSO-BH z1	723.3	61.7	0.30	**741.7**	73.5	73.2	769.8	65.7
CSO-BH z2	654.4	43.6	0.27	**659.7**	50.9	44.3	703.7	47.0
CSO-BH z3	576.8	34.0	0.17	**579.9**	38.2	33.6	636.0	37.6
CSO-BH z4	714.4	57.3	0.26	**732.8**	69.9	68.6	764.7	61.5
CSO-BH z6	689.4	56.5	0.16	**699.6**	74.9	60.4	749.8	61.5
CSO-BH(sz) z1	585.4	41.7	0.20	**586.5**	47.7	40.2	641.5	45.8
CSO-BH(sz) z2	657.7	51.4	0.17	**663.0**	63.9	52.2	717.0	56.2
CSO-BH(sz) z3	675.6	51.2	0.09	**686.3**	67.9	54.8	743.9	56.4
Weighted means:	**640.5**	24.2					715.8	18.6
NH: 842 ± 53 ka (0.927)								
CSO-NH5 z1	878.5	71.0	0.29	**885.4**	99.1	74.8	926.0	75.0
CSO-NH5 z2	821.1	52.5	0.19	**828.4**	58.7	55.2	878.4	56.3
CSO-NH5 z3	816.3	65.0	0.20	**820.5**	71.2	66.0	872.5	69.6
CSO-NH5 z4	816.1	56.0	0.57	**815.1**	63.0	53.3	841.3	57.9
CSO-NH5 z5	873.5	48.6	0.17	**888.1**	68.1	54.9	932.9	52.1
CSO-NH5 z6	829.5	60.4	0.19	**836.4**	69.2	63.5	886.8	64.7
Weighted means:	**839.4**	23.5					889.6	14.1
MB-B: 907 ± 66 ka (0.006)								
CSO-MB-B z1	783.4	45.9	0.17	**788.9**	42.2	51.6	843.1	49.6
CSO-MB-B z2	841.9	45.3	0.15	**843.3**	47.2	46.5	903.5	48.8
CSO-MB-B z3	943.6	53.8	0.22	**942.9**	60.3	51.2	997.5	57.0
CSO-MB-B z4	886.8	54.9	0.14	**896.2**	49.9	64.0	949.0	58.9
CSO-MB-B z5	1062.1	83.6	0.21	**1067.4**	98.4	87.4	1117.1	88.0
CSO-MB-B z6	966.7	77.7	0.17	**964.7**	87.3	76.1	1026.3	82.6
MB z8	1026.8	64.9	0.17	**1030.1**	72.7	65.9	1086.0	68.9
MB z9	1000.8	63.4	0.17	**1003.6**	70.3	63.6	1060.5	67.3
Weighted means:	**906.8**	33.8					997.9	35.6
BL: 942 ± 65 ka (0.044)								
CSO-BL-1 z2	939.5	58.8	0.22	**942.8**	66.2	58.5	993.5	62.4
CSO-BL-1 z3	1041.9	64.6	0.52	**1047.8**	83.9	63.4	1070.8	66.6
CSO-BL-1 z4	983.4	71.1	0.20	**989.8**	94.3	74.6	1040.1	75.3
CSO-BL-1 z5	1056.5	77.1	0.21	**1101.2**	79.5	109.5	1111.9	81.3
CSO-BL-1 z6	978.9	70.0	0.23	**986.7**	85.4	75.7	1032.6	74.0
CSO-BL-1 zR2	943.4	67.0	0.21	**949.0**	73.4	71.0	998.6	71.0
CSO-BL-1 zR4	782.1	50.5	0.34	**779.7**	55.2	47.3	825.0	53.3
CSO-BL-1 zR5	1046.2	85.7	0.18	**1107.4**	73.7	140.4	1104.3	90.6
CSO-BL-1 zR6	924.3	82.1	0.26	**925.5**	87.3	82.6	974.5	86.7
CSO-BL-1 zR7	857.5	57.0	0.23	**858.1**	63.2	56.9	910.4	60.6
CSO-BL-1 zR8	1047.4	94.6	0.31	**1093.3**	89.5	139.0	1093.3	98.8
Weighted means:	**939.1**	27.6					1014.1	27.7
MB-M: 964 ± 46 ka (0.871)								
CSO-MB-M z4	1049.2	80.0	0.24	**1047.1**	87.0	77.5	1101.5	84.3
CSO-MB-M z5	966.9	56.6	0.21	**963.0**	63.8	52.5	1022.2	60.3
CSO-MB-M z6	921.4	63.2	0.22	**917.1**	69.9	58.5	975.6	67.2
CSO-MB-M z7	994.8	69.5	0.17	**992.1**	76.3	65.7	1054.2	74.0
CSO-MB-M z8	933.5	54.2	0.21	**940.1**	50.7	60.9	988.7	57.8
CSO-MB-M z9	937.6	64.3	0.19	**944.7**	60.2	71.7	994.9	68.5
CSO-MB-M z10	944.3	66.0	0.20	**938.6**	74.2	60.3	1000.6	70.3
CSO-MB-M z11	1033.9	73.1	0.21	**1031.8**	80.3	70.6	1089.2	77.3
Weighted means:	**964.9**	22.8					1028.4	16.9
PD: 1640 ± 37 ka								
CSO-PD2 z4	**1597.1**	117.0					1651.5	121.2

(*continued*)

	Secular eq. assumed (U-Th)/He	1σ	D230	Combined U-Pb / U-Th and (U-Th)/He	+1s	−1s	Full diseq. assumed (U-Th)/He	1σ
CSO-PD2 z5	**1601.5**	121.3					1658.9	125.9
CSO-PD2 z6	**1649.5**	135.5					1698.1	139.7
CSO-PD2 z7	**1696.7**	116.4					1756.3	120.7
CSO-PD2 z8	**1664.5**	146.9					1715.9	151.7
Weighted means:	**1640.3**	37.2					1696.1	21.5
NM: 1865 ± 87 ka								
CSO-NM1 z1	**1856.9**	129.7					1924.3	135.1
CSO-NM1 z2	**1947.8**	125.9					2012.9	130.8
CSO-NM1 z3	**1886.6**	137.7					1952.9	143.2
CSO-NM1 z4	**1761.5**	99.2					1827.7	103.7
CSO-NM1 z5	**2068.1**	160.2					2133.3	165.9
CSO-NM1 z6	**1807.9**	135.5					1874.1	141.1
Weighted means:	**1865.5**	87.2					1954.2	48.5

Concordant eruption ages with 2σ uncertainty and goodness of fit parameter (in brackets) are recorded next to the sample names.

References

Braun, J., van der Beek, P., Batt, G., 2012. Quantitative Thermochronology: Numerical Methods for the Interpretation of Thermochronological Data. Cambridge University Press (272 pp).

Casta, L., 1980. Les formation quaternaires de la depression de Brasov (Roumaine). Université d'Aix Marseille II (PhD Thesis Thesis).

Chalot-Prat, F., Gîrbacea, R., 2000. Partial delamination of continental mantle lithosphere, uplift-related crust-mantle decoupling, volcanism and basin formation: a new model for the Pliocene-Quaternary evolution of the southern East-Carpathians, Romania. Tectonophysics 327, 83–107.

Ciulavu, D., Dinu, C., Szakács, A., Dordea, D., 2000. Neogene kinematics of the Transylvanian basin (Romania). AAPG Bull. 84 (10), 1589–1615.

Cloetingh, S.A.P.L., Burov, E., Matenco, L., Toussaint, G., Bertotti, G., Andriessen, P.A.M., Wortel, M.J.R., Spakman, W., 2004. Thermo-mechanical controls on the mode of continental collision in the SE Carpathians (Romania). Earth Planet. Sci. Lett. 218 (1–2): 57–76. https://doi.org/10.1016/S0012-821X(03)00645-9.

Clynne, M.A., Muffler, L.J.P., 2010. Geologic map of Lassen Volcanic National Park and Vicinity, California. U.S. Geological Survey Scientific Investigations Map 2899 (scale 1: 50,000).

Connor, C.B., McBirney, A.R., Furlan, C., 2006. What Is the Probability of Explosive Eruption at a Long-dormant Volcano? School of Geosciences Faculty and Staff Publication, p. 1041

Csontos, L., Nagymarosy, A., Horváth, F., Kovác, M., 1992. Tertiary evolution of the Intra-Carpathian area: a model. Tectonophysics 208 (1–3), 221–241.

Danišík, M., Shane, P., Schmitt, A.K., Hogg, A., Santos, G.M., Storm, S., Evans, N.J., Keith Fifield, L., Lindsay, J.M., 2012. Re-anchoring the late Pleistocene tephrochronology of New Zealand based on concordant radiocarbon ages and combined 238U/230Th disequilibrium and (U–Th)/He zircon ages. Earth Planet. Sci. Lett. 349–350: 240–250. https://doi.org/10.1016/j.epsl.2012.06.041.

Danišík, M., Schmitt, A.K., Stockli, D.F., Lovera, O.M., Dunkl, I., Evans, N.J., 2017. Application of combined U-Th-disequilibrium/U-Pb and (U-Th)/He zircon dating to tephrochronology. Quat. Geochronol. 40:23–32. https://doi.org/10.1016/j.quageo.2016.07.005.

Downes, H., Seghedi, I., Szakács, A., Dobosi, G., James, D.E., Vaselli, O., Rigby, I.J., Ingram, G.A., Rex, D., Pécskay, Z., 1995. Petrology and geochemistry of late Tertiary/Quaternary mafic alkaline volcanism in Romania. Lithos 35, 65–81.

Farley, K.A., 2002. (U-Th)/He dating: techniques, calibrations, and applications. Rev. Mineral. Geochem. 47 (1):819–844. https://doi.org/10.2138/rmg.2002.47.18.

Farley, K.A., Wolf, R.A., Silver, L.T., 1996. The effects of long alpha-stopping distances on (U-Th)/He ages. Geochim. Cosmochim. Acta 60 (21):4223–4229. https://doi.org/10.1016/S0016-7037(96)00193-7.

Farley, K.A., Kohn, B.P., Pillans, B., 2002. The effects of secular disequilibrium on (U–Th)/He systematics and dating of Quaternary volcanic zircon and apatite. Earth Planet. Sci. Lett. 201 (1):117–125. https://doi.org/10.1016/S0012-821X(02)00659-3.

Fielitz, W., Seghedi, I., 2005. Late Miocene–Quaternary volcanism, tectonics and drainage system evolution in the East Carpathians, Romania. Tectonophysics 410 (1–4): 111–136. https://doi.org/10.1016/j.tecto.2004.10.018.

Fillerup, M.A., Knapp, J.H., Knapp, C.C., Raileanu, V., 2010. Mantle earthquakes in the absence of subduction? Continental delamination in the Romanian Carpathians. Lithosphere 2 (5):333–340. https://doi.org/10.1130/L102.1.

Gamble, J.A., Price, R.C., Smith, I.E.M., McIntosh, W.C., Dunbar, N.W., 2003. 40Ar/39Ar geochronology of magmatic activity, magma flux and hazards at Ruapehu volcano, Taupo Volcanic Zone, New Zealand. J. Volcanol. Geotherm. Res. 120 (3):271–287. https://doi.org/10.1016/S0377-0273(02)00407-9.

Ghalamghash, J., Mousavi, S.Z., Hassanzadeh, J., Schmitt, A.K., 2016. Geology, zircon geochronology, and petrogenesis of Sabalan volcano (northwestern Iran). J. Volcanol. Geotherm. Res. 327:192–207. https://doi.org/10.1016/j.jvolgeores.2016.05.001.

Gîrbacea, R., Frisch, W., 1998. Slab in the wrong place: lower lithospheric mantle delamination in the last stage of Eastern Carpathians subduction retreat. Geology 26, 611–614.

Girbacea, R., Frisch, W., Linzer, H.-G., 1998. Post-orogenic uplift-induced extension: a kinematic model for the Pliocene to recent tectonic evolution of the Eastern Carpathians (Romania). Geol. Carpath. 49 (5), 315–327.

Harangi, S., 2001. Neogene to Quaternary volcanism of the Carpathian–Pannonian Region — a review. Acta Geol. Hung. 44, 223–258.

Harangi, S., 2007. A Kárpát-Pannon térség legutolsó vulkáni kitörései - lesz-e még folytatás? (The last volcanic eruptions in the Carpathian-Pannonian Region - to be continued?). Földrajzi Közlemények 131 (4), 271–288.

Harangi, S., Lenkey, L., 2007. Genesis of the Neogene to Quaternary volcanism in the Carpathian-Pannonian region: role of subduction, extension, and mantle plume. Geol. Soc. Am. Spec. Pap. 418:67–92. https://doi.org/10.1130/2007.2418(04).

Harangi, S., Downes, H., Thirlwall, M., Gméling, K., 2007. Geochemistry, petrogenesis and geodynamic relationships of Miocene calc-alkaline volcanic rocks in the Western Carpathian Arc, Eastern Central Europe. J. Petrol. 48 (12):2261–2287. https://doi.org/10.1093/petrology/egm059.

Harangi, S., Molnár, M., Vinkler, A.P., Kiss, B., Jull, A.J.T., Leonard, A.G., 2010. Radiocarbon dating of the last volcanic eruptions of Ciomadul volcano, Southeast Carpathians, Eastern-Central Europe. Radiocarbon 52 (2–3), 1498–1507.

Harangi, S., Sági, T., Seghedi, I., Ntaflos, T., 2013. Origin of basaltic magmas of Perşani volcanic field, Romania: a combined whole rock and mineral scale investigation. Lithos 180–181 (0):43–57. https://doi.org/10.1016/j.lithos.2013.08.025.

Harangi, S., Lukács, R., Schmitt, A.K., Dunkl, I., Molnár, K., Kiss, B., Seghedi, I., Novothny, Á., Molnár, M., 2015a. Constraints on the timing of Quaternary volcanism and duration of magma residence at Ciomadul volcano, east–central Europe, from combined U–Th/He and U–Th zircon geochronology. J. Volcanol. Geotherm. Res. 301:66–80. https://doi.org/10.1016/j.jvolgeores.2015.05.002.

Harangi, S., Novák, A., Kiss, B., Seghedi, I., Lukács, R., Szarka, L., Wesztergom, V., Metwaly, M., Gribovszki, K., 2015b. Combined magnetotelluric and petrologic constrains for the nature of the magma storage system beneath the Late Pleistocene Ciomadul volcano (SE Carpathians). J. Volcanol. Geotherm. Res. 290:82–96. https://doi.org/10.1016/j.jvolgeores.2014.12.006.

Hildenbrand, A., Marques, F.O., Costa, A.C.G., Sibrant, A.L.R., Silva, P.F., Henry, B., Miranda, J.M., Madureira, P., 2012. Reconstructing the architectural evolution of volcanic islands from combined K/Ar, morphologic, tectonic, and magnetic data: the Faial Island example (Azores). J. Volcanol. Geotherm. Res. 241–242:39–48. https://doi.org/10.1016/j.jvolgeores.2012.06.019.

Hora, J.M., Singer, B.S., Wörner, G., 2007. Volcano evolution and eruptive flux on the thick crust of the Andean Central Volcanic Zone: 40Ar/39Ar constraints from Volcán Parinacota, Chile. Geol. Soc. Am. Bull. 119 (3–4):343–362. https://doi.org/10.1130/B25954.1.

Horváth, F., Bada, G., Szafián, P., Tari, G., Ádám, A., Cloetingh, S., 2006. Formation and deformation of the Pannonian Basin: constraints from observational data. Geol. Soc. Lond. Mem. 32 (1):191–206. https://doi.org/10.1144/gsl.mem.2006.032.01.11.

Hourigan, J.K., Reiners, P.W., Brandon, M.T., 2005. U-Th zonation-dependent alpha-ejection in (U-Th)/He chronometry. Geochim. Cosmochim. Acta 69 (13): 3349–3365. https://doi.org/10.1016/j.gca.2005.01.024.

Ianovici, V. and Rădulescu, D. 1966. Geological map 1:200000 L-35-XIV, sheet 20 Odorhei. Geological Institute of Romania, Bucharest.

Ismail-Zadeh, A., Matenco, L., Radulian, M., Cloetingh, S., Panza, G., 2012. Geodynamics and intermediate-depth seismicity in Vrancea (the south-eastern Carpathians): current state-of-the art. Tectonophysics 530–531:50–79. https://doi.org/10.1016/j.tecto.2012.01.016.

Karátson, D., Telbisz, T., Harangi, S., Magyari, E., Dunkl, I., Kiss, B., Jánosi, C., Veres, D., Braun, M., Fodor, E., Biró, T., Kósik, S., von Eynatten, H., Lin, D., 2013. Morphometrical and geochronological constraints on the youngest eruptive activity in East-Central Europe at the Ciomadul (Csomád) lava dome complex, East Carpathians. J. Volcanol. Geotherm. Res. 255:43–56. https://doi.org/10.1016/j.jvolgeores.2013.01.013.

Karátson, D., Wulf, S., Veres, D., Magyari, E.K., Gertisser, R., Timar-Gabor, A., Novothny, Á., Telbisz, T., Szalai, Z., Anechitei-Deacu, V., Appelt, O., Bormann, M., Jánosi, C., Hubay, K., Schäbitz, F., 2016. The latest explosive eruptions of Ciomadul (Csomád) volcano, East Carpathians — a tephrostratigraphic approach for the 51–29 ka BP time interval. J. Volcanol. Geotherm. Res. 319:29–51. https://doi.org/10.1016/j.jvolgeores.2016.03.005.

Kis, B.-M., Ionescu, A., Cardellini, C., Harangi, S., Baciu, C., Caracausi, A., Viveiros, F., 2017. Quantification of carbon dioxide emissions of Ciomadul, the youngest volcano of the Carpathian-Pannonian Region (Eastern-Central Europe, Romania). J. Volcanol. Geotherm. Res. https://doi.org/10.1016/j.jvolgeores.2017.05.025.

Kiss, B., Harangi, S., Ntaflos, T., Mason, P.R.D., Pál-Molnár, E., 2014. Amphibole perspective to unravel pre-eruptive processes and conditions in volcanic plumbing systems beneath intermediate arc volcanoes: a case study from Ciomadul volcano (SE Carpathians). Contrib. Mineral. Petrol. 167 (3):1–27. https://doi.org/10.1007/s00410-014-0986-6.

Klemetti, E.W., Grunder, A.L., 2008. Volcanic evolution of Volcán Aucanquilcha: a long-lived dacite volcano in the Central Andes of northern Chile. Bull. Volcanol. 70 (5): 633–650. https://doi.org/10.1007/s00445-007-0158-x.

Konečný, V., Kovác, M., Lexa, J., Šefara, J., 2002. Neogene evolution of the Carpatho-Pannonian region: an interplay of subduction and back-arc diapiric uprise in the mantle. European Geophysical Union Stephan Mueller Special Publication Series vol. 1, pp. 105–123.

Koulakov, I., Zaharia, B., Enescu, B., Radulian, M., Popa, M., Parolai, S., Zschau, J., 2010. Delamination or slab detachment beneath Vrancea? New arguments from local earthquake tomography. Geochem. Geophys. Geosyst. 11 (3). https://doi.org/10.1029/2009gc002811.

Lindsay, J.M., Trumbull, R.B., Schmitt, A.K., Stockli, D.F., Shane, P.A., Howe, T.M., 2013. Volcanic stratigraphy and geochemistry of the Soufrière Volcanic Centre, Saint Lucia with implications for volcanic hazards. J. Volcanol. Geotherm. Res. 258:126–142. https://doi.org/10.1016/j.jvolgeores.2013.04.011.

Lukács, R., Guillong, M., Schmitt, A.K., Molnár, K., Harangi, Sz., Bachmann, O., 2018. LA-ICP-MS and SIMS U-Pb and U-Th zircon geochronology of Late Pleistocene lava domes of the Ciomadul Volcanic Dome Complex (Eastern Carpathians). Data Brief (submitted).

Martin, M., Wenzel, F., CALIXTO, W.G., 2006. High-resolution teleseismic body wave tomography beneath SE-Romania – II. Imaging of a slab detachment scenario. Geophys. J. Int. 164 (3):579–595. https://doi.org/10.1111/j.1365-246X.2006.02884.x.

Mason, P.R.D., Downes, H., Seghedi, I., Szakács, A., Thirlwall, M.F., 1995. Low-pressure evolution of magmas from the Calimani, Gurghiu and Harghita Mountains, East Carpathians. Acta Vulcanol. 7 (2), 43–52.

Mason, P.R.D., Downes, H., Thirlwall, M., Seghedi, I., Szakács, A., Lowry, D., Mattey, D., 1996. Crustal assimilation as a major petrogenetic process in east Carpathian Neogene to Quaternary continental margin arc magmas. J. Petrol. 37, 927–959.

Mason, P.R.D., Seghedi, I., Szakács, A., Downes, H., 1998. Magmatic constraints on geodynamic models of subduction int he East Carpathians, Romania. Tectonophysics 297, 157–176.

Moriya, I., Okuno, M., Nakamura, E., Szakács, A., Seghedi, I., 1995. Last eruption and its 14C age of Ciomadul volcano, Romania. Summaries of Researches Using AMS at Nagoya University vol. 6, pp. 82–91.

Moriya, I., Okuno, M., Nakamura, T., Ono, K.A.S., Seghedi, I., 1996. Radiocarbon ages of charcoal fragments from the pumice flow deposits of the last eruption of Ciomadul volcano, Romania. Summaries of Researches Using AMS at Nagoya University vol. VII(3), pp. 252–255.

Mucek, A.E., Danišík, M., de Silva, S.L., Schmitt, A.K., Pratomo, I., Coble, M.A., 2017. Post-supereruption recovery at Toba Caldera. Nat. Commun. 8, 15248. https://doi.org/10.1038/ncomms15248.

Nakamura, N., 1974. Determination of REE, Ba, Fe, Mg, Na and K in carbonaceous and ordinary chondrites. Geochim. Cosmochim. Acta 38 (5):757–775. https://doi.org/10.1016/0016-7037(74)90149-5.

Oncescu, M.C., Burlacu, V., Anghel, M., Smalbergher, V., 1984. Three-dimensional P-wave velocity image under the Carpathian arc. Tectonophysics 106 (3):305–319. https://doi.org/10.1016/0040-1951(84)90182-3.

Panaiotu, C.G., Vişan, M., Ţugui, A., Seghedi, I., Panaiotu, A.G., 2012. Palaeomagnetism of the South Harghita volcanic rocks of the East Carpathians: implications for tectonic rotations and palaeosecular variation in the past 5 Ma. Geophys. J. Int. 189 (1): 369–382. https://doi.org/10.1111/j.1365-246X.2012.05394.x.

Peccerillo, A., Taylor, S.R., 1976. Geochemistry of eocene calc-alkaline volcanic rocks from the Kastamonu area, Northern Turkey. Contrib. Mineral. Petrol. 58 (1):63–81. https://doi.org/10.1007/bf00384745.

Pécskay, Z., Szakács, A., Seghedi, I., Karátson, D., 1992. Contributions to the geochronology of Mt. Cucu volcano and the South Harghita (East Carpathians, Romania). Földtani Közlöny 122 (2–4), 265–286.

Pécskay, Z., Lexa, J.A.S., Balogh, K., Seghedi, I., Konecny, V., Kovács, M., Márton, E., Kaliciak, M., Széky-Fux, V., Póka, T., Gyarmati, P., Edelstein, O., Rosu, E., Zec, B., 1995. Space and time distribution of Neogene-Quaternary volcanism in the Carpatho-Pannonian Region. In: Downes, H., Vaselli, O. (Eds.), Neogene and Related Magmatism in the Carpatho-Pannonian Region. Acta Vulcanologica, pp. 15–28.

Pécskay, Z., Lexa, J., Szakács, A., Seghedi, I., Balogh, K., Konecný, V., Zelenka, T., Kovacs, M., Póka, T., Fülöp, A., Márton, E., Panaiotu, C., Cvetkovic, V., 2006. Geochronology of Neogene magmatism in the Carpathian arc and intra-Carpathian area. Geol. Carpath. 57 (6), 511–530.

Peltz, S., Vajdea, E., Balogh, K., Pécskay, Z., 1987. Contributions to the geochronological study of the volcanic processes int he Calimani and Hargitha Mountains (East Carpathians, Romania). Dari de Seama ale Sedintelor Institutul de Geologie si Geofizica 72-73, 323–338.

Popa, M., Radulian, M., Szakács, A., Seghedi, I., Zaharia, B., 2012. New seismic and tomography data in the southern part of the Harghita Mountains (Romania, Southeastern Carpathians): connection with recent volcanic activity. Pure Appl. Geophys. 169 (9):1557–1573. https://doi.org/10.1007/s00024-011-0428-6.

Reiners, P.W., 2005. Zircon (U-Th)/He thermochronometry. Rev. Mineral. Geochem. 58 (1):151–179. https://doi.org/10.2138/rmg.2005.58.6.

Royden, L., Horváth, F., Rumpler, J., 1983. Evolution of the Pannonian Basin system: 1. Tectonics. Tectonics 2 (1):63–90. https://doi.org/10.1029/TC002i001p00063.

Schmitt, A.K., 2011. Uranium series accessory crystal dating of magmatic processes. Annu. Rev. Earth Planet. Sci. 39 (1):321–349. https://doi.org/10.1146/annurev-earth-040610-133330.

Schmitt, A.K., Stockli, D.F., Hausback, B.P., 2006. Eruption and magma crystallization ages of Las Tres Vírgenes (Baja California) constrained by combined $^{230}Th/^{238}U$ and (U–Th)/He dating of zircon. J. Volcanol. Geotherm. Res. 158 (3–4):281–295. https://doi.org/10.1016/j.jvolgeores.2006.07.005.

Schmitt, A.K., Stockli, D.F., Niedermann, S., Lovera, O.M., Hausback, B.P., 2010. Eruption ages of Las Tres Vírgenes volcano (Baja California): a tale of two helium isotopes. Quat. Geochronol. 5 (5):503–511. https://doi.org/10.1016/j.quageo.2010.02.004.

Seghedi, I., Downes, H., 2011. Geochemistry and tectonic development of Cenozoic magmatism in the Carpathian–Pannonian region. Gondwana Res. 20 (4):655–672. https://doi.org/10.1016/j.gr.2011.06.009.

Seghedi, I., Szakács, A., Udrescu, C., Stoian, M., Grabari, G., 1987. Trace element geochemistry of the South Hargitha volcanics (East Carpathians): calc-alkaline and shoshonitic association. Dari de Seama ale Sedintelor Institutul de Geologie si Geofizica 72-73, 381–397.

Seghedi, I., Balintoni, I., Szakács, A., 1998. Interplay of tectonics and neogene post-collisional magmatism in the intracarpathian region. Lithos 45 (1–4):483–497. https://doi.org/10.1016/S0024-4937(98)00046-2.

Seghedi, I., Downes, H., Szakács, A., Mason, P.R.D., Thirlwall, M.F., Rosu, E., Pécskay, Z., Marton, E., Panaiotu, C., 2004. Neogene-Quaternary magmatism and geodínamics in the Carpathian-Pannonian region: a synthesis. Lithos 72, 117–146.

Seghedi, I., Maţenco, L., Downes, H., Mason, P.R.D., Szakács, A., Pécskay, Z., 2011. Tectonic significance of changes in post-subduction Pliocene–Quaternary magmatism in the south east part of the Carpathian–Pannonian Region. Tectonophysics 502 (1–2): 146–157. https://doi.org/10.1016/j.tecto.2009.12.003.

Seghedi, I., Popa, R.-G., Panaiotu, C.G., Szakács, A., Pécskay, Z., 2016. Short-lived eruptive episodes during the construction of a Na-alkalic basaltic field (Perşani Mountains, SE Transylvania, Romania). Bull. Volcanol. 78 (10):69. https://doi.org/10.1007/s00445-016-1063-y.

Siebert, L., Simkin, T., Kimberly, P., 2011. Volcanoes of the World. University of California Press (568 pp).

Singer, B.S., 2014. A Quaternary geomagnetic instability time scale. Quat. Geochronol. 21: 29–52. https://doi.org/10.1016/j.quageo.2013.10.003.

Sperner, B., Lorenz, F., Bonjer, K., Hettel, S., Muller, B., Wenzel, F., 2001. Slab break-off - aprupt cut or gradual detachment? New insights from the Vrancea Region (SE Carpathians, Romania). Terra Nova 13, 172–179.

Sun, S.-s., McDonough, W.F., 1989. Chemical and isotopic systematics of oceanic basalts: implications for mantle composition and processes. Geol. Soc. Lond., Spec. Publ. 42 (1):313–345. https://doi.org/10.1144/gsl.sp.1989.042.01.19.

Szabó, C., Harangi, S., Csontos, L., 1992. Review of neogene and quaternary volcanism of the Carpathian-Pannonian region: a review. Tectonophysics 208, 243–256.

Szakács, A., Seghedi, I., 1986. Chemical diagnosis of the volcanics from the southeastern-most part of the Harghita Mountains — proposal for a new nomenclature. Rev. Roum. Géol. 30, 41–48.

Szakács, A., Seghedi, I., 2013. The relevance of volcanic hazard in Romania: is there any? Environ. Eng. Manag. J. 12, 125–135.

Szakács, A., Seghedi, I., Pécskay, Z., 1993. Pecularities of South Hargitha Mts. as the terminal segment of the Carpathian Neogene to Quaternary volcanic chain. Revue Roumaine de Géologie Géophysique et Géographie, Géologie 37, 21–37.

Szakács, A., Ioane, D., Seghedi, I., Rogobete, M., Pécskay, Z., 1997. Rates of migration of volcanic activity and magma output along the Calimani-Gurghiu-Harghita volcanic range. East Carpathians, PANCARDI'97. Prz. Geol. 45 (10/2), 1106.

Szakács, A., Seghedi, I., Pécskay, Z., 2002. The most recent volcanism in the Carpathian-Pannonian Region. Is there any volcanic hazard? Geologica Carpathica Special Issue, Proceedings of the XVIIth Congress of Carpathian-Balkan Geological Association vol. 53, pp. 193–194

Szakács, A., Seghedi, I., Pécskay, Z., Mirea, V., 2015. Eruptive history of a low-frequency and low-output rate Pleistocene volcano, Ciomadul, South Harghita Mts., Romania. Bull. Volcanol. 77 (2):1–19. https://doi.org/10.1007/s00445-014-0894-7.

Upton, G., Cook, I., 1996. Understanding Statistics. Oxford University Press.

Vaselli, O., Minissale, A., Tassi, F., Magro, G., Seghedi, I., Ioane, D., Szakács, A., 2002. A geochemical traverse across the Eastern Carpathians (Romania): constraints on the origin and evolution of the mineral water and gas discharges. Chem. Geol. 182, 637–654.

Vinkler, A.P., Harangi, S., Ntaflos, T., Szakács, A., 2007. A Csomád vulkán (Keleti-Kárpátok) horzsaköveinek közettani és geokémiai vizsgálata - petrogenetikai következtetések. Földtani Közlöny 137 (1), 103–128.

Wenzel, F., Lorenz, F.P., Sperner, B., Oncescu, M.C., 1999. Seismotectonics of the Romanian Vrancea Area. In: Wenzel, F., Lungu, D., Novak, O. (Eds.), Vrancea Earthquakes: Tectonics, Hazard and Risk Mitigation: Contributions From the First International Workshop on Vrancea Earthquakes, Bucharest, Romania, November 1–4, 1997. Springer Netherlands, Dordrecht:pp. 15–25 https://doi.org/10.1007/978-94-011-4748-4_2.